Optimization of Plastic Scintillator Thicknesses for Online Beta Detection in Mixed Fields

By

Khadijeh Kathy Pourtangestani

A Thesis Submitted in Partial Fulfillment

Of the Requirements for the Degree of

Master of Science

In

Faculty of Energy Systems and Nuclear Science

Program

University of Ontario Institute of Technology

December, 2010

Abstract

For efficient beta detection in a mixed beta gamma field, Monte Carlo simulation models have been built to optimize the thickness of a plastic scintillator, used in whole body monitor. The simulation has been performed using MCNP/X code and different thicknesses of plastic scintillators ranging from 150 to 600 μm have been used. The relationship between the thickness of the scintillator and the efficiency of the detector has been analyzed. For 150 μm thickness, an experimental investigation has been conducted with different beta sources at different positions on the scintillator and the counting efficiency of the unit has been measured. Evaluated data along with experimental ones have been discussed. A thickness of 300 μm to 500 μm has been found to be an optimum thickness for better beta detection efficiency in the presence of low energy gamma ray.

Key words: Plastic Scintillation Detectors, Monte Carlo Radiation Transport, MCNPX code, Efficiency, whole body monitor, Beta/Gamma Mixed Field

Table of Contents

Acknowledgement

I would like to offer my gratitude to Dr. Rachid Machrafi, for his supervision, advice, and guidance from the very early stage of this research as well as giving me extraordinary experiences throughout the work. He provided me with unflinching encouragement and support in various ways. His truly scientific intuition has made him as a constant oasis of ideas and passions, which exceptionally inspire and enrich my growth as a student, a researcher and scientist.

I gratefully acknowledge Greg Bogorodzki, CANBERRA Co., for his advices, supervision, and crucial contribution, which made him a backbone of this research and so to this thesis. During my research time in CANBERRA Co., I have received great help from my colleagues and I am very grateful for their assistance and advices.

Special thanks to MITAC-Accelerate for their generous funding in support of this thesis and much appreciation goes to Dr. Alison Lee for her extraordinary support.

I would like to dedicate this work to my beloved sister, Maryam for her encouragement to achieve my goal by her unsparingly and generously support and to my parents for their unconditional love. And I owe a great debt of gratitude and love to my children, Pouria and Melody, for their patience and understanding perception which has been the best motivation for me.

Lastly, I offer my regards and blessings to all of those who supported me in any respect during the completion of the project, especially to my best friend Azade Tasbaz.

List of Figures

List of Tables

List of Appendices

Acronyms

TPS	Thin Plastic Scintillation
MCNP	Monte Carlo N- Particles
MCNPX	Monte Carlo N Particle Extended
PMT	Photomultiplier Tube
IAEA	International Atomic Energy Agency
ICRP	International Commission on Radiological Protection
ICRU	International Commission on Radiation Units
ISO	International Organization for Standardization

Nomenclature

$h\nu$	Scattered photon energy from the photoelectric effect
$m_o c^2$	Rest energy of the electron, 0.511 MeV
S	Specific energy loss
dE	Differential energy loss
dx	Differential path length
V	Velocity
e	Charge of electron
N	Number density
Z	Atomic number
C	Speed of light
β	Ratio of V/C
$(\frac{dE}{dX})_r$	Radiative energy loss
$(\frac{dE}{dX})_c$	Collisional energy loss

Chapter 1: Introduction

For many years, ionizing radiation has been beneficial to human beings for medical diagnosis and therapy, scientific research, and for generating electrical power [1]. However, when used in unsafe ways, ionizing radiation can harm people and care must be taken to properly use radiation and minimize unnecessary radiation exposures. With the continuous development of nuclear technology and the application of radioactive materials in many different areas of human life, there has been an increased awareness that risks associated with related materials and activities have to be considered and managed to ensure the safety of nuclear workers, environment, and general public.

Within North America, there are large quantities of nuclear material that have been accumulated for many years. For example, spent reactor fuel is stored at nuclear sites, waste is transported to storage areas, and other radioactive materials are used for non-destructive testing and cancer treatments. New materials are produced for the medical industry and shipped to hospitals and to different facilities. Recognizing that evaluating and managing radiation safety required a multidisciplinary technical effort, the field of radiation detection technology was born [2].

Radiation detectors can be used as area monitors in nuclear facilities, and in power plants, they can be placed in vehicles and storage areas that contain radioactive sources to ensure that the containers are properly closed and secure. Further they can monitor areas in medical facilities to ensure that radioactive tracers are properly stored and secured.

Radiation detectors are manufactured in different shapes and size, but their principle relies on the interaction of different types of radiation with the material of the detector. Every detection system operates on a similar principle: it starts with the interaction of the radiation with the

detection medium and then the result of such interaction is transformed into signals, for readout or recorded for further analysis.

Today, tools for detecting ionizing radiation were, in principle, in existence rather early: the phenomenon of thermo-luminescence was first described in the 17th century [3]; the gold leaf electroscope was invented in the 18th century; and photography was developed during the early 19th century. However many years passed until the doors to these completely new fields of science were opened by W.C. Rontgen in 1895, and by H. Becquerel in 1896.

Many reliable instruments for detecting and measuring ionizing radiation are now available, ranging from instruments that are widely used as routine tools in nuclear laboratories, to highly sophisticated and complex instrument systems designed for very special applications such as explosive detection. Detectors have been used not only for investigating the nature of nuclear radiation and radiation emitters, but they have served the beneficial application of radiation in medicine, industry, fundamental research, and also the control of any hazards that might arise from ionizing radiation.

There are a variety of detectors with their strengths and weaknesses. The most recent class of detectors developed are solid state type detectors. These types of devices convert the incident photons directly into electrical pulses. The best detector for a given application depends on several factors (high efficiency, high resolution, ability to operate at room temperature, etc...). Among all detectors, scintillation detectors are very sensitive because of their higher density where the radiation is more likely to be absorbed and detected. They can also resolve the relative energies of the radiation being detected (high resolution) [2].

Probably the earliest example of the use of scintillator sensors, for particle detection, was the spinthariscope invented by Crookes in 1903[5]. This instrument consisted of a ZnS screen

which produced weak scintillations when struck by α particles. When viewed by a microscope in darkened room, they could be discerned even with the naked eye. In 1944 not quite a half century later, Curran and Baker resuscitated the instrument by replacing the human eye with the newly developed photomultiplier tube. The weak scintillations could now be counted with an efficiency and reliability equal to that of the gaseous ionization instruments. Thus was born the modern electronic scintillation detector. New development and improvements followed rapidly so that by the mid-1950's scintillation detectors were among the most reliable and convenient available instrumentation [(8)].

In general, a good scintillator detector should satisfy several requirements, namely, high efficiency for the conversion of incident energy to fluorescent radiation, transparency to its fluorescent radiation so as to allow transmission of the light, emission in a spectral range consistent with the spectral response of existing photomultipliers (PMTs), acceptable energy resolution to identify different energies and finally a short decay constant,τ.

Recently, due to their favorable characteristics compared with other radiation sensors, there has been an increased interest in using plastic scintillators in radiation detection and measurements despite their relatively low sensitivity.

In practice, there is no radiation detector that satisfies all these requirements at once. For example, because of statistical effects, there is no detector with ideal energy resolution, and detector with high resolution such, high pure germanium detector, suffers in terms of sensitivity. Each radiation detector finds a particular application in the detection, identification and sometime in imaging. Thus, in practice, some compromise has to be done and one selects a detector that satisfies as many of the above requirements as possible to the highest degree

possible and, depending on the objective of the measurement, applies appropriate correction to the measured data [7].

Another issue that radiation detection faces is that we are constantly bathed in radiation coming from a variety of natural and artificial sources. These include cosmic rays, radioactive isotopes found naturally in the environment (e.g., the ground, building materials, etc.), nuclear fallout, medical diagnostics, and radioactive sources used in industry which make different complex mixed fields. These fields can be composed by radiation of different nature. Mixed beta/gamma radiation and neutron/gamma fields present good examples encountered in different radiation facilities.

Considering the experimental measurement of the operational dose equivalent quantities in those mixed fields, some practical problems appear as it is usually difficult to measure the dose equivalent with a single detector. This difficulty is due to the different sensitivities, implying different calibration factors for each field component, or to the different measurement conditions required, such as in measurement of penetrating and non-penetrating radiation. Among the situations and activities in which mixed radiation fields are found, specific work-places in nuclear power plants can be cited, as well as other activities related to the nuclear fuel cycle and around medical and research accelerators, in civil and military flights at high altitude and in conditions which exist in the exploration of outer space [9].

For a plastic scintillator, generally used in a large volume detector, the mixed field of beta/gamma radiation has a big influence on their functionality and operation. This organic scintillation material has a low mean atomic number. As a consequence, for gamma radiation, the dominant interaction process is through Compton-scattering so that the main feature in the energy-loss spectrum that is produced, when for example, a 662 keV photon from ^{137}Cs interacts in a 4 cm thick slab of this material, is the Compton-edge at around 450 keV and a

continuum extending into low energies. It is evident that in normal circumstances, such detectors are not suitable for the analysis of the spectra emitted by radioactive source with a view to identifying the isotope and therefore, it is used as a counting detector. Furthermore, its scintillation efficiency is poor compared with other materials and it is difficult to collect this light efficiently from the large-volume detectors. Nevertheless, this material has proved to be very useful in detecting low levels of radiation since it is possible to manufacture large-volumes at relatively low-cost. In fact, the majority of cargo portal-monitors, a big part of full body and tools/object contamination monitors, currently in use for primary screening purposes, are based on scintillation material. However, the portal manufacturers have not maximized either the light-collection efficiency of their detectors nor to optimize the spatial-uniformity of their response. Achieving the greatest sensitivity, whilst maintaining cost-effectiveness, seems to have been their main goal.

Researchers have been studying fundamental characteristics of plastic scintillators such as [4, 8, 9]:

- In-depth examination of Bremsstrahlung and backscatter response characteristics of the detector since a clear understanding of backscattering effects is essential to an accurate correction of the measured data.
- The travel range of the electron inside the scintillation layer is directly proportional to the incident beam energy. Therefore very thin scintillators will not be able to accommodate high energies
- Faster pulse light decay to use in timing applications, even though they often offer little energy resolution.

- The detection efficiency for electrons (beta radiation) is essentially 100% for most scintillators. Since electrons can make large angle scattering, they can exit the detector without depositing their full energy in it. Organic scintillators, having a lower *Z* than inorganic crystals, are therefore best suited for the detection of low-energy (< 10 MeV) electrons [8]

From a manufacturing point of view, there are a few worldwide companies which produce plastic scintillation, such as SAINT-GOBAIN and ELJEN Technology [10]; their products have a maximum wave length emission λ around 425nm with relatively large light output-typically 25-30% of NaI (TI) – and a short decay time of around a few nanoseconds. This makes the material suited for fast timing measurements. All plastic scintillators are sensitive to different types of radiation: X-ray, gamma rays, fast neutrons and charged particles, they can be shaped and fabricated in large volume [10]. In the literature, a recent study by CANBERRA Co. has evaluated the capability of thin plastic scintillation (TPS) detectors for the best beta response possible along with minimizing the gamma response.

To date, the elimination of counting gas has been the only advantage of using plastic scintillation detectors over traditional gas flow detectors in whole body monitors. The sacrifice for this advantage was in detector performance (low efficiency, bad uniformity) leading to longer counting time. The need for counting gas has been eliminated by using scintillation detectors with an embedded PMT to minimize dead space between detectors. The TPS detectors in the Argos-PB models (Appendix B) are also a brand new design. Their design has been optimized to provide excellent signal-to-noise ratios and furthermore, the detection capability both across and along the detectors is extremely uniform, but still has challenge because of its low efficiency [11].

The phoswich detector is used for the detection of low-level radiation in the presence of considerable background. It consists of two different scintillators coupled together and

mounted on a single photomultiplier tube. By utilizing the difference in the decay constants of the two phosphors, differentiation between events taking place in the two detectors is possible. The combination of different kind of scintillation layers is under investigation [11] and this work presents a part of this investigation by CANBERRA Co. Scintillators can be operated as beta spectrometers, providing the energy distribution of the beta radiation with excellent discrimination of the photon component, whose contribution has to be determined by a different instrument. Currently, thin plastic scintillators are facing many challenges:

- Methods for filtering gamma events and unwanted direct interactions in the photodiode are needed [14].
- Thin-layered scintillators at specific density depth will be invaluable for expansion of the prototypes into fast and efficient beta dosimeter measurements.
- Higher energy betas easily pass completely through the thin plastic scintillator with little energy deposition and some produce Cerenkov light in the light pipe. Very energetic Compton electrons from higher energy photon interactions in the detector or light pipe also can produce Cerenkov light. These are problems associated with very thin plastic scintillator detectors that otherwise would not be of as much concern for thicker detectors [9].
- Light output: Only a small fraction of the kinetic energy lost by a charged particle in a scintillator is converted into fluorescent light. The remainder is dissipated non radiatively, primarily in the form of lattice vibrations and heat. The fraction of energy that is converted into fluorescence energy (scintillation efficiency) depends on the particle type and its energy.
- Relative dosimetry, very thin plastic scintillators (thickness <0.5 mm) can be used for absolute dosimetry if calibrated appropriately. Precautions of which users should be

aware include, but are not limited to: errors in the estimation of dose rate at the reference point in fields where there is a significant variation of absorbed dose rate within the volume of the detector, change of sensitivity with time due to radiation damage of the scintillator and/or its associated light guides, change in the sensitivity of the light-collection system, and changes in the background signal due to ambient light leakage [7].

The use of a plastic scintillator with optimum thicknesses for beta/gamma radiation detection is an approach where the physics and techniques are solidly established. The current work "*Optimization of Plastic Scintillator Thicknesses for Beta Detection in Mixed Fields*" represents a part of few projects that CANBERRA Co. proposed for collaboration with the University of Ontario Institute of Technology in the frame of an internship program for graduate students, and it consists of identifying suitable scintillators and optimizing their thicknesses to develop beta/gamma detectors. These systems will have broad-ranging applications in nuclear non-proliferation, radioactive waste management, nuclear worker monitoring, system reliability, dose assessment, and risk analysis. The improvement of such devices is crucial; since it is related not only to security issues but also to respond to the strict requirements of national and international regulatory bodies (they required strict specification on norms and standards for radiation detector designers).

In the light of this, CANBERRA Company, as a large worldwide company manufacturing radiation instruments using plastic scintillators of different kind in a big part of its products, launches a further investigation to improve the performance and ISO standard functionality of its products. One of the CANBERRA products using a plastic scintillator is the "Argos full body monitor" [11]. The monitor uses several units composed of thin plastic scintillators (see details later). However with the current configuration and layer thickness, for detecting beta radiation, the system has low detection efficiency and consequently long counting time is

required. In the beginning of this study, the idea was to optimize the system for detecting beta and gamma radiation, however the task was enormous and it was reduced to investigate the beta radiation component of the system and leave the remaining part of the task for further investigation.

In this study, a thin plastic scintillator was characterized by simulating its response functions by means of detailed Monte Carlo simulations as well as by experimental investigation of its response to beta and gamma radiation at fixed energies. The latter results were used to obtain a better understanding and validation of the MCNP simulations. Tests were also conducted at the CANBERRA facility in order to compare the results with simulations of the response in a mixed radiation beta/gamma field. It is demonstrated that these detectors can be characterized sufficiently enough to serve their function as radiation monitors.

The objective of this thesis is to determine some of the parameters of the recently designed unit cell of a full body monitor Argos-TPS and to optimize the plastic scintillator thickness for better efficiency of the unit for beta detection. More specifically, the study aims to:

1. To characterize the parameters of the monitor and determine its efficiency as a function of the position where the incident radiation falls on the detector
2. Increase the beta detection efficiency of the unit to reduce the monitoring time by keeping the gamma contamination component at lowest level possible
3. Find an optimum layer thickness for multitask detection system that can include gamma radiation in future design

This thesis contains an introduction, four chapters, conclusion, appendices, and a list of references. The introduction presents a general description of the work, the challenges that radiation detection is currently facing and it formulates the objectives of the thesis.

Chapter 1 gives a general background on gamma and beta interactions with matter, radiation detection using scintillation detectors in particular plastic scintillators. Chapter 2 presents the experimental data measured with different sources at different sites where the unit was deployed. To quantify the characteristics of the unit, chapter 3 describes in details the MCNP simulation models that have been built in this work and the methodology adopted for the simulation. Chapter 4 is dedicated to discuss the results obtained both in the simulation and in experiments. The thesis ends with a conclusion where the main results have been drawn with recommendation for next generation of detector units.

Chapter 2: General Background on Beta/Gamma Radiation Interaction and Detection

Radiation interaction is the mechanisms by which ionizing radiation interacts and loses energy as it moves through matter. Because the detection of radiation is based on its interaction and on the amount of energy deposited in the material of which the detector is made, the study of this subject is extremely important for radiation measurement and protection. Thus, to be able to improve the detectors' functions and interpret the results of the measurement, one needs to know how radiation interacts and what the consequences are of the various interactions [5]. The current work deals only with beta and gamma interactions with matter particularly their interactions with plastic scintillators. The operation of any radiation detector basically depends on the manner in which the radiation to be detected interacts with the material of the detector itself. An understanding of the response of a specific type of detector must therefore be based on a familiarity with the fundamental mechanisms by which radiations interact and lose their energy in the detector media.

Among all the detectors, plastic scintillators exhibit very short response time and are extensively used for experiments where accurate measurements of very short time intervals at the level of nanosecond must be obtained in spite of prodigiously high count rates. Other common applications of plastic scintillators are when large volume detectors are needed, for example, multiple-detectors arrays for whole body monitors in nuclear facilities and when dealing with the detection of charged particles with minimal response to gamma-rays. These plastic scintillators give a great practical value because they can be made into rigid masses of very clear material of any size or shape desired. All plastic scintillators are sensitive to X-rays, gamma rays, fast neutrons and charged particles. Plastic scintillators offer high

performance, ease of handling, and mechanical stability at a relatively lower cost when compared to inorganic scintillators such as NaI, CsI or LaBr crystals[8].

Ionizing radiations interact with the scintillator, which almost immediately converts some of the absorbed energy into a flash of light. The scintillator is generally mounted directly on a photomultiplier tube (PMT) when a small sample of the scintillator is used. But when a large volume is required, generally, the PMT is housed in a light guide pipe which transfers the photons from the scintillator to the photocathode of the PMT. The Photocathode is a translucent, light sensitive coating of material on the PMT window, when it absorbs light it emits a proportional number of electrons. The section below describes different interaction mechanisms of beta and gamma radiation with matter.

2.1. Interaction of gamma with matter

The behavior of photons in matter is dramatically different from that of charged particles. The photon's lack of an electric-charge makes impossible the many inelastic collisions with atomic electrons so characteristic of charged particles. The main interactions of photons (X-ray and γ-rays) with matter are:

1. Photoelectric absorption
2. Compton scattering and,
3. Pair production.

These modes of interactions explain the two principal qualitative features of photons: (1) they are many times more penetrating in matter than charged particles, and (2) a beam of photons is not degraded in energy as it passes through a thickness of matter, but only attenuated in intensity[4].

Two of these mechanisms, *photoelectric absorption* and *Compton scattering*, predominate in the case where the energy of the gamma-ray does not greatly exceed 1.02 MeV. In the case of higher-energy photons, *pair production*, which is a direct conversion of electromagnetic energy into mass, occurs. These three gamma-ray interaction mechanisms result in the release of electrons in the absorber. Photoelectric absorption predominates for low-energy gamma rays (up to several hundred keV), pair production predominates for high-energy gamma rays (above 5-10 MeV), and Compton scattering is the most probable process over the range of energies between these two extremes [(4)]. The atomic number of the interaction medium has a strong influence on the relative probabilities of these three interactions, such that there is a preference on choosing detectors for gamma-ray spectroscopy for materials that incorporate elements with high atomic number[(6)].

2.1.1. Photoelectric absorption

In this mode of interaction, a photon interacts with an absorber atom and the photon completely disappears. The photon energy dislodges a *photoelectron* from one of the atom bound shells Fig.2.1. The interaction is with the atom as a whole, with an individual electron, but one that is tightly bound, and cannot take place with a free electron. The most probable origin of the photoelectron is from the most tightly bound K shell. The photoelectron energy is given by equation [1] [(5)],

$$E_e = h\nu - E_b \qquad [1]$$

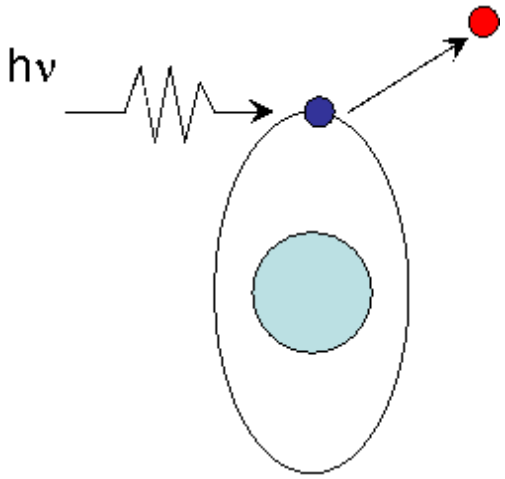

Fig.2.1. Incident photon interacts with a tightly bound electron

Where E_b is the binding energy of the photoelectron in its original shell and hν is the energy of the incident gamma. Moreover, the photoelectric interaction leaves an ionized absorber atom with a vacancy in one of its orbital shells. By capturing a free electron from the medium or rearrangement of electrons from other shells of the atom, this vacancy is rapidly filled. The rearrangement of electrons may generate one or more characteristic X-rays. Additionally, the probability of this interaction increases for absorber materials of high atomic number.

2.1.2. Compton effect

In this interaction mechanism, the incident gamma ray photon is scattered, by interacting with an electron, through an angle θ with respect to its original direction (Fig.2.2).

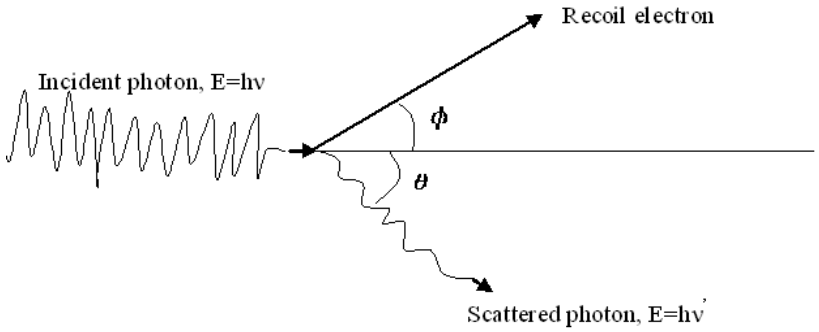

Fig.2.2. Recoil electron and scattered photon in the Compton scattering process

Differing from the photoelectric process, only a portion of the photon energy is transferred to the electron, known as a recoil electron. The energy transferred to the recoil electron can vary from zero to a large fraction of the incident gamma ray energy. By writing simultaneous equations for conservation of energy and momentum, equation [2] can be derived.

$$h\nu' = \frac{h\nu}{1 + \frac{h\nu}{m_0 c^2 (1 - \cos\theta)}} \qquad [2]$$

Where m_0c^2 is the rest energy of the electron (0.511 MeV), from the above equation, the scattered photon has its maximum energy at θ = 0 where $h\nu = h\nu'$, and has its minimum energy at θ = π where $h\nu = h\nu / (1+2h\nu/ m_0c^2)$.

2.1.3. Pair production

Based on Einstein's theory of relativity, when a high-energy (>1.022 MeV) photon interacts with the strong electromagnetic field surrounding a nucleus, as illustrated in Fig.2.3, the

photon energy can be converted into a pair of electron masses, one of which is negatively charged (the electron) and the other is positively charged (the positron).

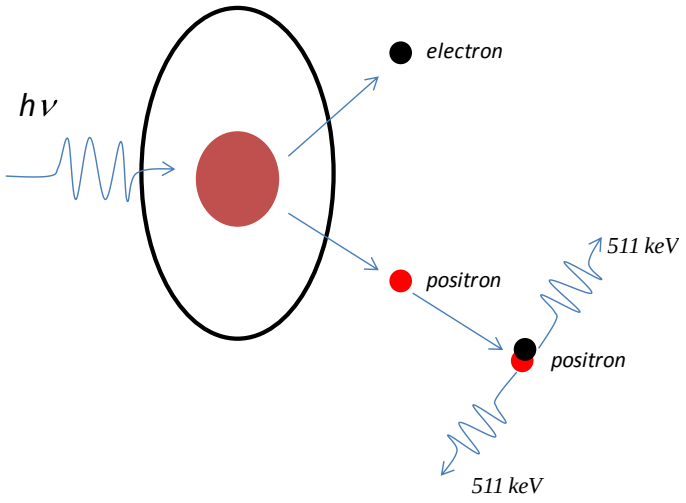

Fig.2.3. Pair production interaction

The positron and electron share the energy remaining after the electron masses have been formed (hν=1.022 MeV). As a practical matter, the probability of this interaction remains very low until the gamma ray energy approaches several MeV, and therefore pair production is predominantly confined to high-energy gamma rays. Eventually, the energy of the positron and electron will be absorbed in the medium and, because the positron will subsequently annihilate after slowing down in the absorbing medium, two annihilation photons (0.511 MeV) (Fig.2.3) with opposite directions are produced.

The relative importance of the three processes described above for different absorber materials and gamma ray energies is conveniently illustrated in Fig.1.4. The line at the left represents the energy at which photoelectric absorption and Compton scattering are equally probable as a function of the absorber atomic number. In particular material like plastic scintillation, with low atomic number (Z, Hydrogen and Carbon), the probability of Compton scattering is the highest one for gamma ray interaction. The preceding analysis is based on

the assumption that Compton scattering involves electrons that are initially free of unbound. In actual detector material, the binding energy of the electron prior to the scattering process can have a measurable effect on the shape of the Compton continuum. These effects will be particularly noticeable for low incident gamma-ray energy [4].

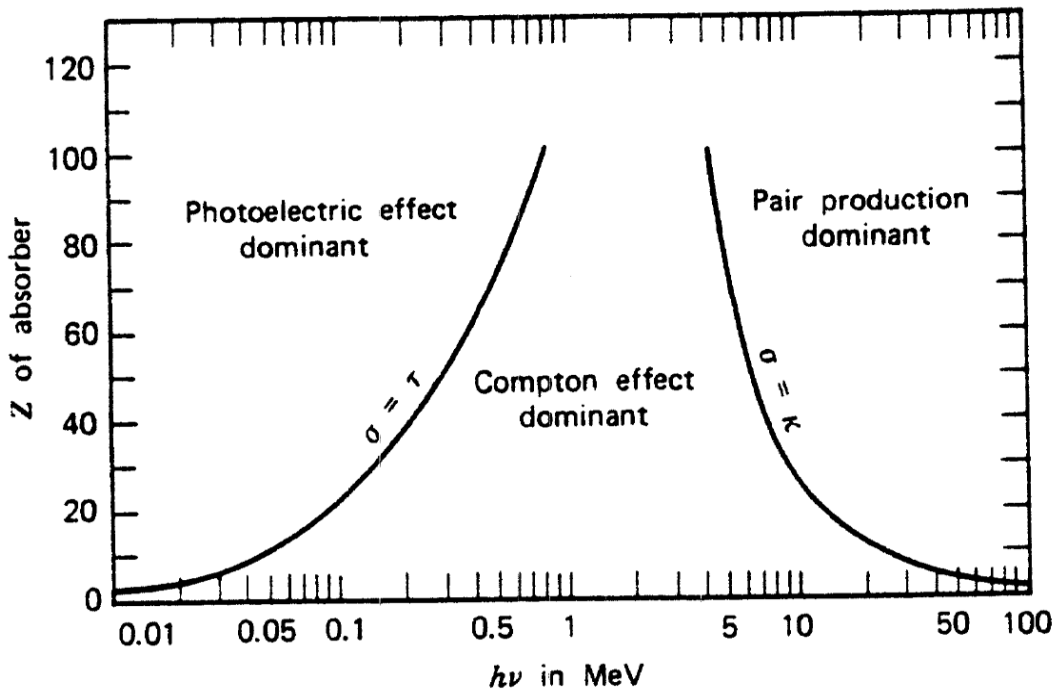

Fig.2.4. Relative importance of the three major types of gamma-ray interaction [5].

2.2. Interaction of beta with matter

Electron interaction is different from either photon or heavy charged particles. Uncharged particles, such as photons, undergo a relatively small number of collisions as they interact with matter. Electrons are charged particles and thus interact continuously through long-range Coulomb force. An electron typically undergoes roughly 10^4 more collisions for the same energy loss than a neutral particle. For example, an electron slowing down from 0.5 MeV to 0.0625 MeV will undergo on the order of 10^5 collisions. A photon needs only about

20-30 Compton scatters to reduce its energy from several MeV to 50 keV [7]. Upon entering any absorbing medium, beta particles immediately interacts simultaneously with many orbital electrons. With any of such encounters, the electron experiences an impulse from the attractive Coulomb force as it passes around the encounter vicinity. Depending on the proximity of the encounter, this impulse may be sufficient either to raise an electron to a higher-lying shell within the absorber atom *(excitation)* or to completely remove the electron from the atom *(ionization).* At any given time, the particle is interacting with many electrons, so the net effect is to decrease its velocity continuously until the particle is stopped [8]. When compared with heavy charged particles, beta particles lose energy at a lower rate and follow a much more tortuous path through absorbing materials. Large deviations in the beta particle path are possible because its mass is equal to that of the orbital electrons with which it is interacting, and a much larger fraction of its energy can be lost in a single encounter[7].

Electrons can lose energy in collisions with atomic electrons, leading to excitation and ionization of the medium. At low electron energies, radiative losses are negligible. The relative importance of ionization to excitation increases rapidly with the energy of the electron. The collisional energy loss for electrons is based on the unrestricted stopping power, which gives the energy loss per unit length in equation [3].

$$S = -\frac{dE}{dx} \qquad [3]$$

Where, S is defined as the differential energy loss (dE) for that particle within the material divided by the corresponding differential path length (dx).

This value is also called the *specific energy loss.* For fast electrons, Equation [4] (Bethe equation) describes the specific energy loss due to ionization and excitation (the "collisional losses").

$$-\left(\frac{dE}{dx}\right)_c = \frac{m_0 v^2 E}{2L^2(1-\beta^2)} - \ln 2\left(2\sqrt{1-\beta^2-1+\beta^2}\right) + \frac{1}{8\left(1-\sqrt{(1-\beta^2)^2}\right)} \qquad [4]$$

In this equation, *v* and *e* represent the velocity and charge of an electron, *N* and *Z* represent the density and atomic number of the absorber atoms, m_0 represents the electron rest mass, β is the ratio of *v/c* (*c* is the speed of light), and the parameter *I* represents the average excitation and ionization potential of the absorber and is normally treated as an experimentally determined parameter for each element [(5)].

Electrons also differ from heavy charged particles in that, energy may be lost by radiative processes as well as by coulomb interactions. These radiative losses take the form of Bremsstrahlung or electromagnetic radiation, which can emanate from any position along the electron track. From classical theory, any charge must radiate energy when accelerated, and the deflections of the electrons in its interactions with the absorber correspond to such acceleration [(5)]. The linear specific energy loss through radiative processes identified by subscript "r" (bremsstrahlung) is,

$$-\left(\frac{dE}{dx}\right)_r = \frac{NEZ(Z+1)e^4}{137 m_0 c^4\left(\frac{4\ln 2E}{m_0 c^2} - \frac{4}{3}\right)} \qquad [5]$$

Where, *E* represents the energy of the particle. The yield from heavy charged particles is negligible as indicated by the presence of the m_0^2 factor in the dominator of the multiplicative term in Equation [5]. The factors of E and Z^2 in the numerator show that radiative losses are most important for high electron energies and for absorber materials of large atomic number. As the electron energy increases, Bremsstrahlung becomes important.

Therefore, the total stopping power for electrons with higher energies is the sum of the collisional and radiative losses:

$$\frac{dE}{dx} = (\frac{dE}{dx})_c + (\frac{dE}{dx})_r \qquad [6]$$

And the ratio of the specific energy losses is approximately given by:

$$\frac{(\frac{dE}{dx})_r}{(\frac{dE}{dx})_c} = \cong \frac{EZ}{700} \qquad [7]$$

For the electrons of interest in our investigation (such as beta particles and secondary electrons from gamma-ray interactions), typical energies are less than 1 MeV. Therefore, radiative losses from typical energy beta particles in absorbers of low atomic number are always a small fraction of the total energy loss.

Because of their mass, beta particles often undergo large angle deflections along their paths. This leads to the phenomenon of backscattering. This effect could remove an entering beta particle from the surface through which it entered. These backscattered electrons do not deposit all their energy in the medium (detector), and therefore the backscattering process can have a significant effect on the response of the detector which been designed to collect electron energy spectra. Beta particles with high incident energy and absorbers with low atomic number have the lowest probability for the backscattering effect [(6)]. In addition, because of its small mass, electrons are particularly susceptible to large angle deflections by scattering from nuclei. This probability is so high, in fact, that multiply scattered electrons may be turned around in direction altogether, so that they are backscattered out of the absorber, this is illustrated schematically in Fig.2.5. The effect is particularly strong for low energy electrons, and increases with the atomic number Z of the material. Backscattering also depends on the angle of incidence. Obviously electrons entering at oblique's angles to the

surface of the absorber have a greater probability of being scattered out than those incident along the perpendicular. Backscattering is an important consideration for electron detectors where depending on the geometry and energy, a large fraction of electrons may be scattered out before being able to produce a usable signal in the detector [8].

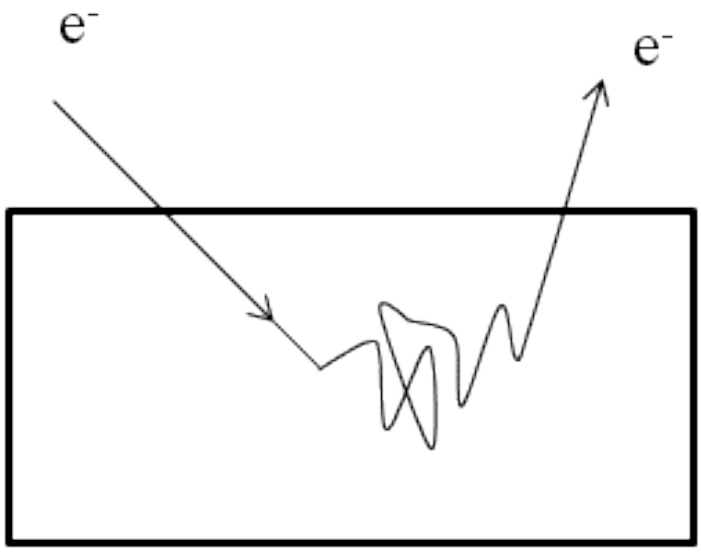

Fig.2.5. Multiple scattered electron

Knowing that charged particles lose their energy in matter, a natural question to ask is: how far will the particles penetrate before they lose all of their energy? Moreover, if we assume that the energy loss is continuous, this distance must be a well defined number, the same for all identical particles with the same initial energy in the same type of material. This quantity is called the range of the particle, and depends on the type of material, the particle type and its energy. For instance, for small thicknesses, most of the particles manage to pass through. The fact is that the energy loss is not continuous, but statistical in nature. A measurement with an ensemble of identical particles show a statistical distribution of ranges centered about some mean value [8].

$$S(T_0) = \int \left(\frac{dE}{dx}\right)^{-1} dE \qquad [8]$$

Where T_0 is the initial energy, this yields the approximate path-length travelled. Equation [8] ignores the effect of multiple Coulomb scattering, which causes the particles to follow a zigzag path through the absorber. Thus, the range, defined as the straight-line thickness, will generally be smaller than the total zigzag path length. Range energy relation is necessary for deciding the sizes of detectors to be used in an experiment or in determining the thickness of radiation shielding [8]. Because of the electron's greater susceptibility to multiple scattering by nuclei, the range of electrons is generally very different from the calculated path length obtained from an integration of the dE/dx formula given in equation [8]. Differences ranging from 20-400% depending on the energy and material are often found. In addition, the energy loss by electrons fluctuates much more than for heavy particle. This is due to the much greater energy transfer per collision allowed for electrons and to the emission of Bremsstrahlung radiation. In both cases, it is possible for a few single collisions to absorb the major part of the electron energy [7].

2.3. Gamma and beta detection

After examining the interaction of beta and gamma radiation with matter, the following section will deal with the detection of these types of radiation.

Most of the detectors used to measure ionizing radiation (such as beta and gamma radiation) are based on the ability of the radiation to ionize materials or to excite atoms within materials. Most of the radiation detectors used in radiation measurement falls into three categories: gas-filled detectors, scintillation detectors, and semiconductor detectors. In the

following paragraphs, we summarized some of them in relationship to the detection of beta and gamma radiations. Many of the differences among the ways in which these radiations interact and what types of detectors are appropriate depend on the fundamental differences among the radiations themselves. Preferably, organic scintillators and particularly, plastic scintillators are the main target for this paper.

2.3.1. Gamma detection

Gamma-ray detectors are devices that transform γ–ray radiation into a measurable electrical current. There are various detector types with different characteristics, depending on detector material. As a response to incident γ-rays, a detector material generates a current, voltage or light pulse. The intensity of the pulse is proportional to the energy deposited by the in the detector. The amount of pulses recorded for a given number of incident γ-ray is expressed in detection efficiency. The higher the efficiency of detection, the shorter the recording time can be. In general, the efficiency of a detector increases with an increase in mass and atomic number of the detector material [(9)]. There is currently a very wide range of scintillating and solid-state materials available for use in gamma-ray detection. The purpose of this brief review is to highlight the key properties of the three main classes of gamma-ray detectors that are currently widely used. Each of these detector types finds particular application in the detection, identification and imaging. The choice of a particular detector type for an application depends upon the gamma energy range of interest, the application, and resolution

and efficiency requirements. Additional considerations include count rate performance, the suitability of the detector for timing experiments, and of course, the price.

2.3.1.1. Plastic Scintillators (Polyvinyltoluene PVT)

This organic scintillation material has a low mean atomic number. As a consequence, the dominant interaction process is through Compton-scattering. Moreover, because of the low Z-value of their constituents (hydrogen, carbon, and oxygen), and loosely bound orbital electrons, there is virtually no photoelectric cross section for gamma rays of typical energies. As we mentioned it before, typical organic scintillators show no photo-peak and will give rise only to a Compton continuum in their gamma-ray pulse height spectrum (to provide some possibility for photoelectric conversion of gamma-rays, by adding high-Z elements to organic scintillators, like lead or tin up to a concentration of 10% by weight [9]. Plastic scintillators have so far been ignored in field applications for gamma-ray measurements, even though they have some practical advantages over inorganic scintillators in terms of being less dense, less expensive, less temperature sensitive, rugged and are manufactured in large machinable volume.

2.3.1.2 Inorganic scintillation

These detectors consist of translucent material. When absorbing γ-radiation, a light pulse is emitted and is detected by a photomultiplier tube (PMT) attached to the detector crystal, which converts the light into an electric signal. Scintillators have a poorer resolution than semi-conductor detectors. However, the average atomic number of inorganic scintillators is generally higher and the crystal sizes can be larger than that of semi-conductor detectors,

leading to higher detection efficiencies and relatively more counts in the full-energy peak. Examples of inorganic scintillators are Alkali Halide Scintillators [NaI (Tl), CsI (Tl) and BGO (Bismuth Germanate or Bi4Ge3O12)] and others.

a. Sodium Iodide

Sodium iodide-based scintillation detectors have, until recently, been the detectors of choice for use in medium-resolution gamma-ray spectroscopy. It is possible to manufacture large volumes of this alkali halide crystal that have a consistent quality. Since the atomic number and density of the material is high, the efficient detection of gamma-radiation in the range up to say 3 MeV can be achieved using crystal thicknesses of 10cm (~80% absorption at 2.0 MeV). This means that the emphasis on increasing detection efficiency has been directed towards the use of as large an area as is possible that is consistent with not degrading the overall spectral-resolution at 662 keV to below ~8%. This has meant that the practical limitation on the area of a detector having this spectral-resolution is currently ~ 400cm^2. Techniques have been developed which can lead to a very significant utilization of the energy-loss spectrum generated by these detectors. The increased number of counts in the peaks, their sharpness and accuracy of location has led to the development of new high-performance isotope-identification systems based on the use of NaI (Tl) scintillators [14].

b. Lanthanum Halides

There has been an important development that is already impacting the quality of the spectra that can now be provided by inorganic scintillation counters. Whilst these new materials ($LaBr_3$ and $LaCl_3$) are currently significantly more expensive than NaI and are generally not available in such large volumes, it is anticipated that they will become much more competitive within the next few years. Nevertheless, $LaBr_3$ is already showing its special

value by improving the ability to improve the quality of isotope-identification that can be achieved without the use of sophisticated software [9].

c. BGO Crystal

BGO (Bismuth Germanate Bi4Ge3O12) is the crystalline form of an inorganic oxide with cubic eulytine structure, colorless, transparent, and insoluble in water. When it is exposed to radiation of high energy particles or gamma-rays, x-rays, it emits a green fluorescent light with a peak wavelength of 480 nm. With its elevated stopping power, high efficiency scintillation, first-rate energy resolution and non-hygroscopes, BGO is an excellent scintillation material and is ideal for a wide range of applications in high energy physics, nuclear physics, space physics, nuclear medicine, geological prospecting and other industries [14].

2.3.1.3. Solid-state detectors

These detectors offer by far, the best spectral-resolution. Their high-resolution is especially important in the identification of the isotopic composition of the source of radiation and in the ability to detect a source in the presence of background.

Most promising of these detectors are those based on the CdTe or CdZnTe. These materials have, until recently, been available in only small volumes (~ few cm^3) but they do have the advantage of being able to provide a spectral-resolution some 30-40% better than $LaBr_3$. These detectors will not play a significant role when a large volume detector is required because of their small size and modest stopping power.

2.3.2. Beta detection

Beta particles are detected through their interaction with matter. One class of detectors employs gas as the detection medium. Ionization chambers, proportional counters, and Geiger-Müller counters are of this class. In these detectors, after entering through a thin window, the beta particles produce positive ions and free electrons as they collide with atoms of the gas in the process of their slowing down. An electric field applied across the volume of gas causes these ions and electrons to drift along the field lines, causing an ionization current that is then processed in external electronic devices. These three original gas devices serve as a good illustration of the application of gas ionization phenomena in this class of instruments. These detectors are actually the same device working under different operating parameters [(6)].

In a semiconductor detector, a solid media replaces the gas. When a beta particle enters the detector, it causes struck electrons to be raised into the conduction band, leaving holes behind in the valence band. The electrons and holes move under the influence of an imposed electric field, causing a pulse of current to flow. Such detectors are useful mainly for low-energy beta particles. A less obvious but fundamental advantage of semiconductor detectors is the fact that much less energy is required (~3eV) to produce a hole-electron pair than that required (~30 eV) to produce an ion electron pair in gases [(7)].

More precise energy information can be achieved with scintillation detectors. In certain substances, the passage of a charged particle through matter temporarily raises electrons in the material into excited states. When these electrons fall back into their normal state, light may be emitted and detected as in the scintillation detector [(8)]. If a clear plastic scintillator is used, it can be mounted on a photomultiplier tube, which converts the transmitted light into a

measurable electrical current pulse whose amplitude is proportional to the energy deposited by the incident beta particle. Scintillation detectors respond to energy absorption from ionizing radiation by emitting light. The light is most often measured with a photomultiplier tube that converts the light to an electronic pulse. These detectors may be either inorganic crystals or organic compounds. All inorganic scintillators rely on the crystalline nature of the material for light production and most have impurity atoms, with ionization potentials less than atoms of the crystal, added as activators. Ionizing radiation may elevate electrons from the conduction band to the valence band of the crystal. The electrons can migrate in the conduction band and holes left in the valence band may also move and ionize a host atom that it encounters. The impurity ions introduce trapping levels in the energy gap between the valence and conduction bands [(4)]. In brief, electrons may move into an excited level of the activator ion and then drop to the ground energy state with the emission of light as shown in Fig.2.6.

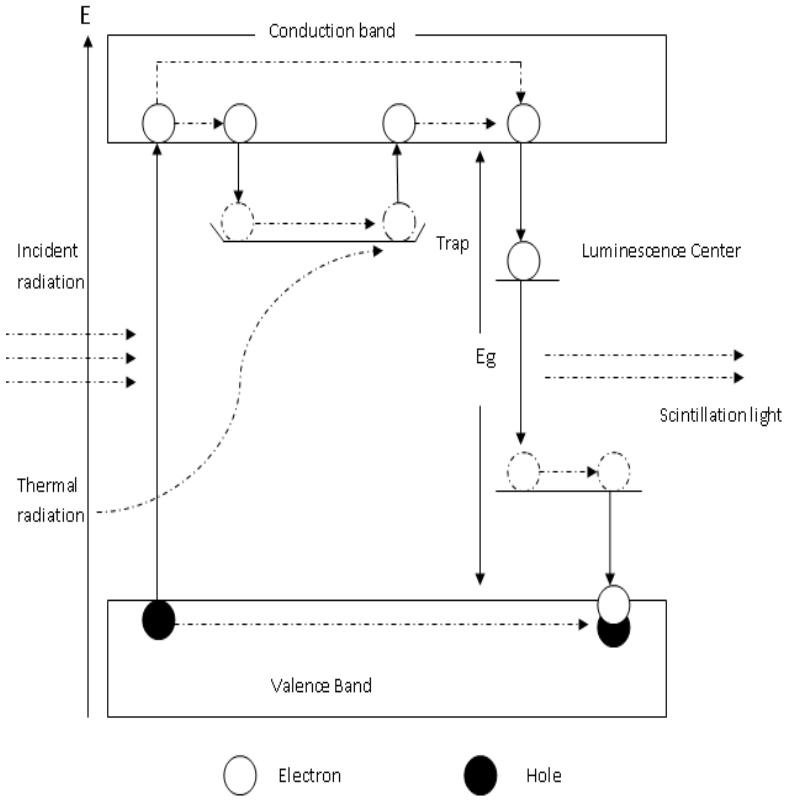

Fig.2.6. Principal of luminescence in a scintillation material

An ideal scintillator should possess the following properties [5]:

- It should convert the kinetic energy of charged particles into detectable light with high scintillation efficiency.
- The conversion should be linear; the light yield should be proportional to deposited energy over as wide a range as possible.
- The medium should be transparent to the wavelength of its own emission for good light collection.
- The decay time of the induced luminescence should be short so that fast signal pulses can be generated.
- The material should be of good optical quality and subject to manufacture in sizes large enough to be of interest as a practical detector.

- Its index of refraction should be near that of glass (~ 1.5) to permit efficient coupling of the scintillation light to a photomultiplier tube.

2.3.2.1. Inorganic scintillators

Most of the inorganic scintillators have crystalline structures. These materials are generally denser and have higher atomic number than organic scintillators. This makes them attractive in applications where high stopping power for the incident radiation is desired. Another advantage is their higher light output than organic scintillators. Inorganic crystalline scintillators such as sodium iodide (NaI), and cesium iodide (CsI) are hygroscopic (rapidly absorb moisture from the air) so they must be sealed in air tight. Because of this they cannot be used to detect betas and they are gamma ray detectors [(14)]. Other inorganic crystalline scintillators, especially sodium iodide activated with thallium, NaI (Tl), have been used for gamma-ray energy measurements. Such detectors can be grown as large single crystals that have a reasonably high efficiency for absorbing all of the energy from incident gamma rays. They are used most often with a photomultiplier tube to convert the light pulses to electronic pulses which are usually sorted, according to pulse height, using a multichannel analyzer. A pulse that represents full energy deposition by a gamma ray in the detector falls in a region of the distribution of pulses called the photo-peak region and can be associated with specific gamma ray energy.

2.3.2.2. Plastic Scintillators (organic)

Organic scintillators are extensively used in radiation detectors. They are found in solid, liquid, and gaseous states. The organic scintillators are aromatic hydrocarbon compounds containing linked or condensed benzene-ring structures. If an organic scintillator is dissolved

in a solvent which can then be subsequently polymerized, the equivalent of a solid solution can be produced. A common example is a solvent consisting of styrene monomer in which an appropriate organic scintillator is dissolved. The styrene is then polymerized to form a solid plastic. They are synthetically produced through a process that is time consuming and highly labor intensive. The base material that is generally used for the mixture is acrylic, polystyrene, or polyvinyl-toluene monomer. A convenient scintillator is then added to this base and mixed homogeneously. The concentration of this main scintillator is about 1% by weight of the mixture, which is sufficient to produce a high light yield. Most manufactures offer different scintillators based on varying concentrations of solvents, so that the user could make the selection according to the system requirements. A plastic scintillator produced by this method has several attractive qualities, such as; chemically stable, high degree of optical homogeneity, and can be cut and machined into virtually any shape. Because the material is relatively inexpensive, plastics are often the only practical choice if large-volume solid scintillators are needed [16]. Their most distinguishing feature is a very rapid decay time on the order of a few nanoseconds or less. The principal scintillation light (or prompt fluorescence) is emitted in transition between higher level and one of the vibration states of the ground electronic state. If τ represents the fluorescence decay time, then the prompt fluorescence I intensity at a time t following excitation should simply be [7]:

$$I(t) = I_0 e^{-\frac{t}{\tau}} \qquad [9]$$

In most organic scintillators, τ represents a few nanoseconds, and the prompt component is relatively fast. Now we know how scintillation light is produced, we will proceed to the discussion of the important parameters related to use of plastic scintillation as radiation

detection device such as: light output, Nonlinearity of light output, time response, uniformity of light collection, reflection, and light pipe.

The light output of a scintillator refers more specifically to its efficiency for converting ionization energy to photons. This is an extremely important quantity, as it determines the efficiency and resolution of the scintillator. Small fraction of the kinetic energy lost by a charged particle in a scintillator is converted into fluorescent energy. The remainder is dissipated non-radiatively, primarily in the form of lattice vibrations or heat. The fraction of the particle energy which is converted (the scintillation efficiency) depends on both the particle type and its energy. The response of organic scintillators to charged particles can best be described by a relation between dL/dx, the fluorescent energy emitted per unit path length, and dE/dx, the specific energy loss for the charged particle. The light output is a strong function of the type of incident particle or photon and of its energy, which therefore strongly influences the type of scintillation material to be used for a particular application.

The major problem associated with plastic scintillators is their nonlinear behavior. The light output per unit length has a nonlinear dependence on the energy loss per unit length of the particles track. This behavior is characterized by the so called Birk's formula [5].

$$\frac{dL}{dX} = \frac{S\frac{dE}{dX}}{1+KB\frac{dE}{dX}} \qquad [10]$$

$\frac{dL}{dX}$ represents the light output per unit length

$\frac{dE}{dX}$ represents the energy lost by the particle per unit length of its path = stopping power, depends on the type of the material and type of the incident radiation, S represents a normal

scintillation efficiency, KB represents an adjustable parameter to fit experimental data for a specific scintillator.

When excited by fast electrons (either directly or from gamma-ray irradiation), dE/dx is small for sufficiently large value of E and Birk's formula then predicts [5]

$$\frac{\mathbf{dL}}{\mathbf{dX_e}} = \mathbf{S}\frac{\mathbf{dE}}{\mathbf{dX}} \qquad [11]$$

Or the incremental light output per unit energy loss is a constant

$$\frac{\mathbf{dL}}{\mathbf{dE_e}} = \mathbf{S} \qquad [12]$$

and

$$L = \int_0^E \frac{dL}{dE} dE = SE \qquad [13]$$

There must be a value of stopping power at which all the molecules have been excited. The sample in this state will be said to have reached a state of saturation. After reaching this state, delivering more energy to the material would not increase the light output, Fig.2.7.

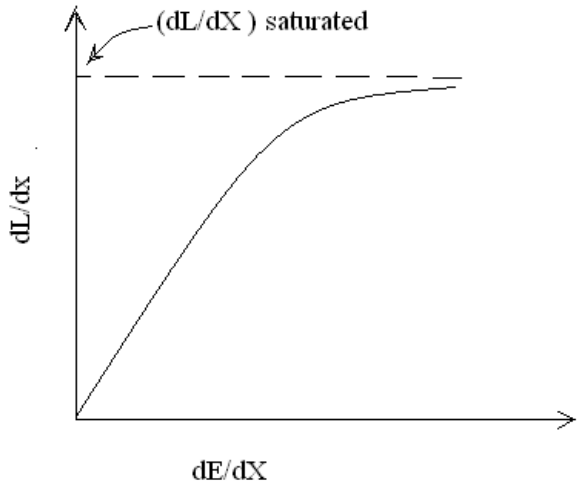

Fig.2.7. Plot of Birk's formula in arbitrary units (Birk- law [4])

The non-proportional response of the typical organic scintillators was studied in comparison to that of a BGO ($Bi_4Ge_3O_{12}$) crystal by A. Nassalski and his colleagues [16] the studies covered tests of BC408 plastic, BC501A liquid scintillator and anthracene organic crystal. The observed non-proportionality of organic scintillators differs a lot from those measured for inorganic crystals. The light yield of inorganic scintillators become proportional at energies above 100 keV, while in the case of organic scintillators it is above 500 keV for anthracene and above several MeV for plastic and liquid scintillators. The observed effect can be related to a strong quenching of the light emission, known for charged particles in organic scintillators, which is much stronger than that observed in inorganic scintillators. The study in this work showed a much larger non-proportionality of the light yield of organic scintillators than that known for most of the inorganic crystals. In the case of anthracene the non-proportionality covers energy range up to about 500 keV, while for the BC408 plastic and BC501 a liquid scintillators, it is above 4 MeV energy, the observed effect can be related to a strong quenching of the light emission, known for charged particles in organic

scintillators, which is much larger than that observed in inorganic scintillators. The larger non-proportionality found for BC408 plastic and BC501A liquid scintillators in comparison to anthracene suggests that the non-proportionality is also affected by the energy transfer process in organic scintillators. According to the present knowledge the non-proportionality of the light yield of scintillators appears to be the fundamental limitation of energy resolution **(12)**.

One of the important differences between inorganic and organic scintillators is in the response time, which is less than 10ns for the latter (response time of inorganic scintillators is almost 1μs) and makes them suitable for fast timing measurements [(16)]. Experimentally, the rise and fall of the light output can be characterized by the full width at half Maximum (FWHM) of the resulting light versus time profile, which can be measured using very fast timing procedures. It is becoming increasingly popular to specify the performance of ultrafast Organic scintillators by their FWHM time rather than the decay time alone. Among these is the finite flight time of the photons from the point of scintillation to the photomultiplier tube [(17)]. Particularly in large scintillators, transit time fluctuation due to multiple light reflections at scintillator surfaces can amount to a sizable spread in the arrival time of the light at the PMT. Also, self absorption and reemission of the fluorescence plays an important role in causing an apparent worsening of the time resolution as the dimensions of a scintillator are increased. The excitation and de-excitation processes in organic scintillators can be described adequately by simple exponential rise and decay times. Rise times are typically very short

(on the order of hundreds of picoseconds) and decay times are typically on the order of 1-4 nanoseconds, dependent on the molecular energy-state structure of the organic. The light output from an organic scintillator can be described by this equation [(4)]

$$I(t) = I_0(e^{-\frac{t}{\tau}} - e^{-\frac{t}{\tau_1}}) \quad [14]$$

Where τ is the decay time constant and τ_1 is the excitation time constant. Other observations have concluded a Gaussian function *f(t)*, the overall light versus time profile is then described by

$$I(t) = I_0 f(t) e^{\frac{t}{\tau}} \quad [15]$$

As we mentioned it before, rise and fall of the light output can be characterized the full width at half maximum (FWHM) of the resulting light versus time profile, which can be measured using very fast timing procedures [(5)].

In any scintillation detector, one would like to collect the largest possible fraction of the light emitted isotropically from the track of the ionizing particle. Two effects arise in practical cases which lead to less than perfect light collection: optical self-absorption within the scintillator and losses at the scintillator surfaces. With the exception of very large scintillators or rarely used scintillation materials (e.g., ZnS), self-absorption is usually not a significant loss mechanism. The uniformity of the light collection will determine the variation in signal pulse amplitude as the position of the radiation interaction is varied throughout the scintillator. Perfect uniformity would assure that all events depositing the same energy, regardless of where they occur in the scintillator.

Because the scintillation light is emitted in all directions, only a limited fraction can travel directly to the surface at which the photo multiplier tube or other sensor is located. The remainder, if it is to be collected, must be reflected one or more times at the scintillator surfaces. The smaller the angle of incident leads to the higher the probability that the photon

will again hit the opposite wall of the container [19]. After one or more such reflections the photons reach the photo-detector and get counted. Because of difficulty to ensure a very high degree of smoothness as any deviation would let the photons wonder around more and even get absorbed by material and even the simple reflection is always associated with some degree of absorption by the material, therefore the intensity of light emitted by the scintillator is bound to decrease as the light travels down the light guide.

The simplest way to transfer scintillation photons from the scintillator to the photo-detector is to directly attach a scintillator to a photo-detector having an area greater than the scintillator to avoid loss of photons. However, the geometries of scintillators and photo-detectors normally do not full-fill this requirement and the situation is the other way round. Hence building a detector in such a configuration is generally not possible. A more practical approach is to use a light guide to connect the photon emitting surface to the photo-detectors such that the scintillation photons reach the photo-detectors with minimal loss. There is different kind of light guide, such as; glass and Plexiglas, fiberglass, clear plastic, and liquid [20]. The light pipes also serve a useful purpose in other situation, if scintillation measurements are to be made in strong magnetic field, the PM tube must be shielded from the field and this often implies its removal to a location some distance away from the scintillator. Very thin scintillators should not be mounted directly on the PM tube end window to avoid the pulse height variations that can arise due to photocathode non-uniformities. A light pipe between the PMT the scintillator will spread the light from each scintillation event over the entire photocathode to average out these non-uniformities. They are generally optically transparent solids with a relatively high index of refraction to minimize the critical angle (the critical angle θ_c is determined by the indices of refraction for the scintillation medium and the surrounding medium, if the angle of incidence θ is greater

than the critical angle θ_c , total internal reflection will occur) for total internal reflection. Surfaces are highly polished and are often surrounded by a reflective wrapping to direct back some of the light that escape at angles less than the critical angle [18].

2.4. Detection of beta and gamma radiation in mixed field

Mixed field are those composed by radiation of different types and /or energy, of photons and electrons with sufficiently different energy. Mixed field can be composed by radiation of different nature but with the same weighting factors, like beta-photon fields for example, which one of the most is frequently found in practice. Among the situation and activities in which mixed fields are found, specific workplace in nuclear power plants can be cited, as well as other activities related to the nuclear fuel cycle. Mixed fields can be found around medical and research high energy accelerators, in civil and military flights at high altitude and in conditions which exist in the exploration of outer space. For example, a ^{137}Cs that is encapsulated may only emit the predominant 662 keV gamma from ^{137m}Ba, but if un-encapsulated material is present, we would expect to have a beta field from the ^{137}Cs betas and conversion electrons. Under some conditions, the energy from an isomeric transition can be transferred to an electron within the atom [19]. This energy supplies the binding energy and expels the electron from the atom. This process is known as internal conversion (IC) and is an alternative to gamma emission. In many nuclides, isomeric transitions produce gamma photons and internal conversion electrons. Examples of gamma emission after beta decay from ^{60}Co and ^{137}Cs radio-nuclides are depicted in Fig.2.8.

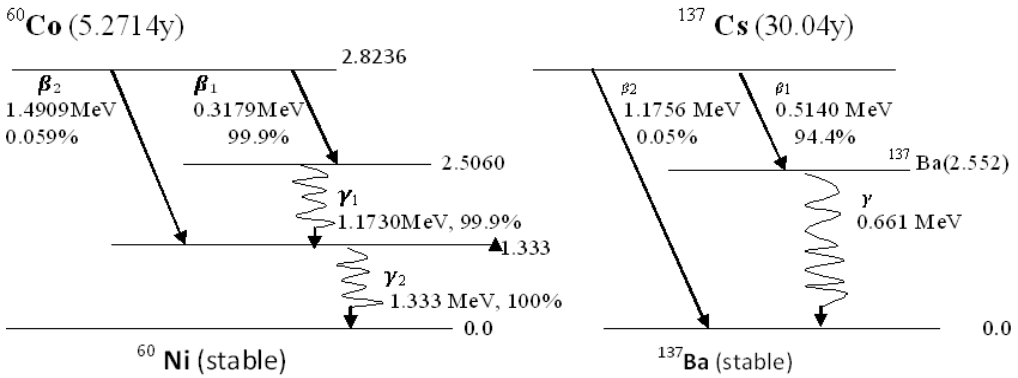

Fig.2. 8. Transformation of ^{60}Co and ^{137}Cs to stable nuclides by beta decay and their immediate gamma-ray emissions

The detection of beta radiation in a mixed field with gamma radiation has been addressed in the 10th conference of IEEE [15]. In this meeting researchers point out that organic scintillators are the best choice due to their nearly-tissue equivalence, thus favoring good energy dependence. Alternatively, scintillators can be operated as beta spectrometers, providing the energy distribution of the beta radiation with excellent discrimination of the photon component, whose contribution has to be determined by a different instrument. The spectroscopic mode is convenient when beta doses are important. The equivalent dose can be accurately computed starting from the spectral distribution by the use of the appropriate values for the mass stopping power. In addition to doses, beta spectrometry also provides useful information, such as the maximum beta energy, which can be used to optimize the protection of exposed workers. Beta spectrometry can also be achieved with semiconductor detectors or by combining both scintillators and semiconductors, assembling thin and thick detectors forming a two-element telescope. However, the superior energy resolution of semiconductors makes them preferable over scintillators for some applications [10]. The operational principle of the telescope type spectrometers is based on the different way photons and betas interact with matter. Betas, interacting via Columbian forces, lose energy

in a continuous way, while photons lose energy by discrete interactions in specific places. Beta radiation will lose some energy in traversing the thin detector producing a pulse while photons likely not if the detector is thin enough. Operating in coincidence the pulses produced simultaneously in both detectors will only be caused by betas, discriminating in this way the photon contribution. The scintillator detector should be thick enough so as to stop all the betas and measure their energy distribution.

The use of phoswich detectors to measure coincident nuclear signatures has proven itself to be a useful technique. From early studies it is clear that matching the two scintillator materials must be done carefully in terms of scintillation light wave-length, pulse time decay, and radiation detection properties. For specific applications, the use of carefully chosen phoswich detectors and pulse-shape analysis techniques can reduce the experimental complexity. This in turn leads to easier operations and less maintenance. The YAP/BGO detector under consideration here performed well as a beta-gamma detector for several radio-xenon isotopes, radon and radon daughter products. Further detector optimization in terms of detector material thickness and geometry will lead to better signature deconvolution and enhanced detection [18]. Plastic scintillator plates sandwiched between thin radioactive samples were viewed with two photomultipliers and the coincident outputs were measured. For β^--rays, the pulse-height distributions showed approximately triangular shapes and the pulse-height endpoints were proportional to their maximum energies. Similar characteristics were also found in the case of γ-rays. The counting efficiencies were empirically determined as functions of radiation energies in both cases.

Recent studies have evaluated the capability of plastic scintillation (PS) as an alternative to liquid scintillation (LS) in radionuclide activity determination without mixed waste production. In order to complete the comparison, we now assess the extent to which PS can

be used to quantify mixtures of radionuclides and the influence of the diameter of the plastic scintillation beads in detection efficiency. The results show that the detection efficiency decreases and the spectrum shrink to lower energies when the size of the plastic scintillation beads increases, and that the lower the energy of the beta particle, the greater the variation takes place. Similar behavior has been observed for beta-gamma and alpha emitters. Two scenarios for the quantification of mixtures are considered, one including two radionuclides (^{14}C and ^{60}Co) whose spectra do not overlap significantly, and the other including two radionuclides (^{137}Cs and $^{90}Sr/^{90}Y$), where the spectra of one the isotopes is totally overlapped by the other.

2.4.1. Gamma energy deposition

Gamma-ray, form of electromagnetic radiation interacts with low-z plastic materials principally by Compton scattering. When a Compton event occurs, electrons recoil up to a maximum energy of $E_e=E\gamma/ (1+mc^2/2E\gamma)$. This is charged particle that will further interact with the scintillator to produce photons [19]. To measure the energy of the incident particle with a scintillator, the relationship between the pulse height and the energy deposited in the scintillator must be known. Because the pulse height is proportional to the light produced by the scintillator, it is necessary to know the light-conversion efficiency of the scintillator as function of the type and energy of incident radiation. The beam of photons is not degraded in energy as it passes through a thickness of matter, only attenuated in intensity. The Compton scattering process, at sufficiently high photon energy, depends only on the number of electrons in the scintillator and not upon the nature of the nuclei. The fraction of photons surviving a distance x in the material is then given by the well known formula of attenuation

$$I(t) = I_0 e^{-\mu x} \qquad [16]$$

Where I_0 represents the incident intensity, μ represents the probability per unit length for an interaction and x represents the traveled distance.

2.4.2 Beta energy deposition

It is necessary to determine the relation between the energy deposited in the medium by incident electrons and the fluorescent yield of an organic plastic scintillator. As we mentioned before, well-known demonstrations of the dependence of the specific light yield on the specific energy loss of the particle leads to the conclusion that L(E) must be nonlinear for low-energy electrons [8].

The energy that is transferred to the orbital electron must come at the expense of the incident electrons and its velocity is therefore decreased as a result of the encounter. The maximum energy that can be transferred from an incident electron of mass m with kinetic energy E to an electron of mass m_0 in a single collision is $4Em_0/m$. Because this is a small fraction of the total energy; the primary electron must loss its energy in many such interactions during its passage through an absorber. At any given time, the incident electron is interacting with many electrons, so the net effect is to decrease its velocity continuously until the incident electron is stopped. Electrons are therefore characterized by a definite range in a given absorber material.

In this work, the loss considered is in thin scintillators**.** For such thin absorbers that are penetrated by a given charged particle, the energy deposited within the absorber can be calculated from [5]

$$\Delta E = (-\frac{dE}{dx})_{avg} x \qquad [17]$$

Where x represetns the absorber thickness and $(-dE/dx)_{avg}$ is the linear stopping power averaged over the energy of the particle while in the absorber. If the energy loss is small, the

stopping power does not change much and it can be approximated by its value at the incident particle energy. The value of –dE/dx along an electron particle track is also called its specific energy loss or, more casually, its rate of energy loss. A plot of the detected number of electrons versus absorber thickness begins to drop immediately and gradually approaches zero for large absorber thicknesses, Fig.2.9. Those electrons that penetrate the greatest absorber thickness will be the ones whose initial direction has changed least in their path through the absorber.

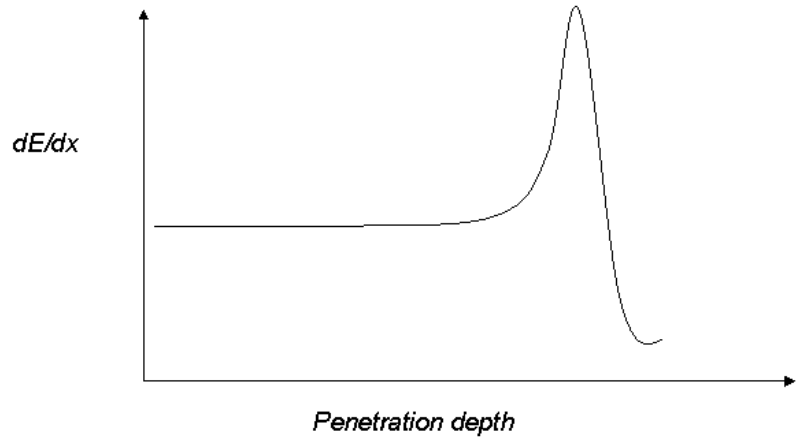

Fig.2.9. Typical Bragg peak showing the variation of dE/dX as a function of the penetration depth of the charged particle in matter (the particle is more ionizing towards the end of its path [4])

The nature of the electron response function depends on the scintillation material, its physical thickness, and the angle of incidence of the electrons. Electrons from an external source normally must pass through some protective covering before reaching the surface of the scintillator itself. The energy loss that may occur in these intervening materials is not explicitly considered but may be important if the electron energy is small and the detector may not be totally opaque to the secondary bremsstrahlung photons that will be generated along the path of the electron. In general, the response functions show a pronounced full-

energy peak corresponding to the total absorption of the incident electron energy, together with a tail extending to lower energies. The major cause of such partial energy absorption is backscattering. Other that contributes to the tail is those electrons which are fully stopped within the scintillator but which generate bremsstrahlung photons that escape from the front or back surface of the detector. Both the probability of backscattering and the fraction of the electron energy loss to bremsstrahlung increase markedly with the atomic number of the scintillator. The scintillator with low atomic number is generally preferred for electron spectroscopy. Therefore, plastic scintillator is most commonly applied in electron measurements.

2.5. Beta/ gamma devices

There is a continuing and growing need for a simple and robust method which can be used to reliably characterize mixed beta/gamma radioactive field in nuclear facility and field environments.

Gamma radiation is quite penetrating and, depending on its energy, can easily pass through rather large thicknesses of materials. Gamma rays can observe by detectors like G-M detector, but the efficiency is much lower than that for beta particles that enter the detector. G-M detectors with relatively thick walls are often used for measuring the intensities of gamma radiation fields. Proportional detectors also respond with low efficiency to gamma radiation, if the voltage is set sufficiently high, but this is not a common application. Ionization chambers are used more for gamma radiation intensity measurements than for beta, although there are ionization chambers that have been designed for beta detection. The most commonly used ionization chambers for gamma measurements use air as the fill gas. They are operated at a low enough voltage so that no multiplication of the original ionization events occurs and only

the ionization produced by those original events is collected. They are frequently used in a mode (called mean level mode) such that the signal from a large number of ionizing events is recorded or measured per unit time rather than attempting to resolve individual pulses. They are commonly used for gamma dose measurements in radiation protection.

Beta detection can also be achieved with semiconductor detectors or by combining both scintillators and semiconductors [17]. The operational principal of this method is based on the different way photons and betas interact with matter. Beta, interacting via columbine forces, loses energy in a continuous way, while photons lose energy by discrete interactions in. Beta radiation will lose some energy in traversing a thin detector producing a pulse while photons likely not if the detector is thin enough. The scintillator detector should be thick enough so as to stop all the betas and measure their energy distribution. Therefore, in mixed field, if we need to detect just beta radiation, the best detector is a thin plastic scintillator. Next chapter discuss a detailed simulation, using MCNPX, to optimize the proper thickness of a plastic scintillator to efficiently detect beta radiation in mixed beta gamma fields.

Chapter 3: Experimental Investigation with Existing Unit

Thin plastic scintillators are the major sensors used in many detectors and monitors manufactured by CANBERRA Co., the Argos-TPS monitor 5PB (Appendix B), recently designed, is using a plastic scintillator of 150μm in thickness. Fig. 3.1 shows a cell unit of the monitor. The purpose of this chapter is to investigate the characteristics of this unit that is intended to detect beta-particles in a mixed beta/gamma radiation fields, namely, we measured the detection efficiency of the unit and the position dependence.

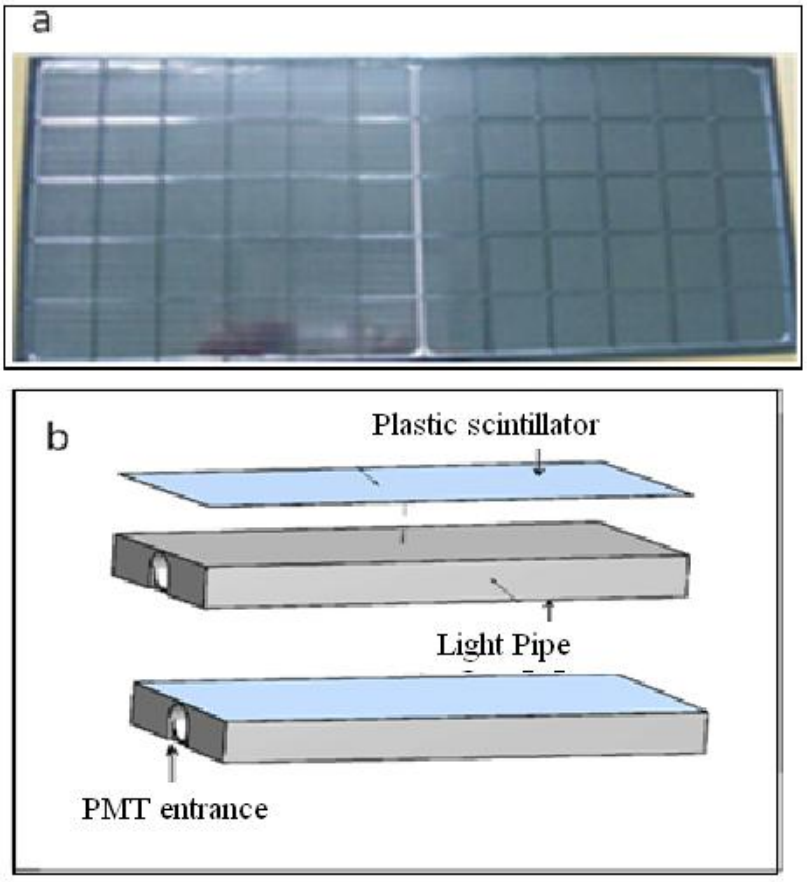

Fig.3.1: Cell unit used in Argos-TPS 5PB
(a) plastic scintillator layer and (b) plastic box showing the PMT insertion

The above cell unit is a fundamental cell of the whole body monitors. As shown in Fig.3.2, the unit is present in different monitors to serve different screening purposes. The unit contains a single PMT for each detector allowing optimization of the operating parameters of the detector. Calibration of all detectors can be accomplished in less than 15 minutes. An electronics module box is connected to the back of each detector and performs amplification, discrimination and providing high voltage. A built in computer manages the system operation automatically. A lockable keyboard interface is used for parameter setting, testing, calibration and maintenance. A separate LED on each detector shows which detector is alarming and/or being addressed on the LCD screen. The computer runs Windows XP Embedded installed on a local industrial grade hard disk drive and can make use of USB flash drive for transferring data. Data may be retrieved either this way or via a LAN connection [11]. For more details about features of Argos-TPS family of whole body contamination monitors, see Appendix B.

Fig.3.2: Argos Two-Step (front, back, side, head, hands and feet) whole body surface contamination monitors.

In spite of many advantages for this unit i.e. fast response, hardness against radiation damages, the light output is lower than expected for the practical purposes of whole body monitoring in the shortest possible time. We have set up an experiment to measure the efficiency after irradiating the unit with beta particles from different sources located at different positions.

3.1. Experimental set up

The detector-unit was tested to ensure that it could, indeed, measure efficiently at the level necessary for a radiation sensor system. A block diagram of the testing system is shown in Fig.3.3. The plastic scintillation detector used during this experiment was EJ-212 (equivalent to BC-400) (see details in Appendix D). It has dimensions of 36.05x15.84x3.53cm^3 and was covered by a black plastic box with a comb window on top. The photomultiplier PMT was optically coupled to one side of the plastic box, beneath the scintillation layer. The unit detector was connected to a computer to count photons every 10 seconds period. Measurements with the detector unit have been performed for different sources that create a mixed beta gamma field. The main goal of this testing was to measure the efficiency of the detector with 150μm thickness for the scintillation layer and, later, to guide the MCNP calculations for better optimization.

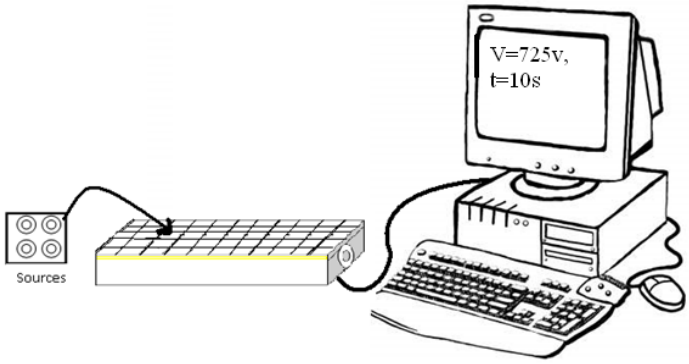

Fig.3.3: Block diagram of the experimental setup

3.2. Experiment with beta sources

The experiment has been carried out by irradiating the detector unit with different sources on different positions on the scintillator. Since this experiment presented the starting point for further improvement of the unit, the unit was divided in different cells as shown in Fig. 3.4 and in each experiment; first step was leading by locating beta sources on each cell and counts the number of event for about 10 seconds for each position.

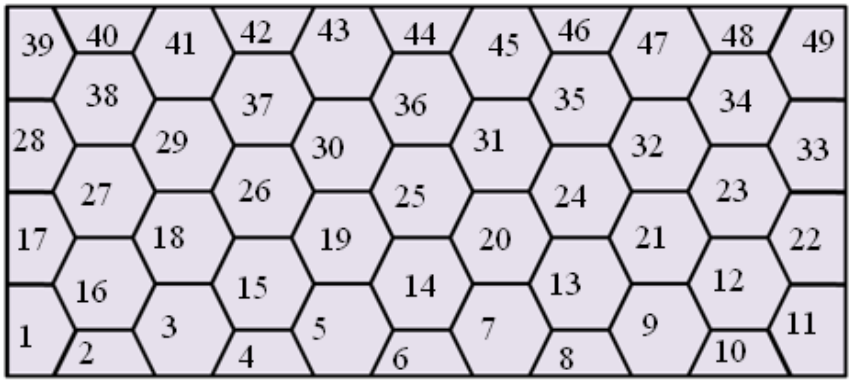

Fig.3.4: Top window combed coverage of detector unit was numbered to indicate the process of the experiment in Canberra site.

Furthermore, testing was repeating by increasing the irradiating time and increasing the distance between the source and detector unit as well. The radiation sources such as ^{14}C, ^{60}Co, ^{137}Cs and ^{36}Cl have been chosen to match the ones encountered at work places where the monitors are deployed. The characteristics of the radiation sources used in the experiment are listed in Table2.1, while the results of the experiments are presented in Table 3.2, 3.3, 3.4, and 3.5.

Table3.1: Characteristics of sources

Element	Radiation type	Energy, MeV	$T_{1/2}$, y	A, Bq	Range , mm
^{14}C	Beta	0.156	5730	39627	0.28
^{60}Co	Beta-gamma	0.334	5.27	7385	1.09
^{137}Cs	Beta-gamma	0.512	30.23	33600	1.78
^{36}Cl	Beta	0.709	$3*10^5$	36914	2.80

3.3. Experimental data

The sensitivity of the TPS, Thin Plastic Scintillation detector, is a fundamental parameter of this detector in the process of radiation monitoring since it is related to the scanning time and to the energy of particles to be detected in ordinary nuclear facility places. Thus, the increase of the detector sensitivity will decrease the risk of being contaminant in these places and therefore improves the safety of the job conditions. This experiment has been done just for one thickness for 150 μm for two reasons: the first one is to guide the further MCNPX simulation and the second one because the unit is a functioning unit at CANBERRA site. Finally we should mention that this test was carried out in a low gamma radiation field, which considerably simplifies the experiment conditions.

Table 3.2: Experimental results after exposing the detector unit to ^{14}C on each cell (CPS=Count Per Second)

Cell #	CPS	Cell #	CPS	Cell #	CPS	Cell #	CPS
1	2002±14	13	1319±12	25	2404±16	37	2034±14
2	1812±14	14	2038±14	26	2107±15	38	2015±14
3	2115±15	15	2137±15	27	2130±14	39	1234±11
4	1796±13	16	2154±15	28	1234±11	40	1460±12
5	2105±15	17	2025±14	29	1367±12	41	1937±14
6	1471±12	18	2165±15	30	1981±14	42	1597±13
7	1435±12	19	2223±15	31	1080±10	43	1898±14
8	1069±10	20	1873±14	32	2091±15	44	1203±11
9	1296±11	21	1301±11	33	1789±13	45	1513±12
10	998±10	22	1070±10	34	1321±12	46	1185±11
11	1113±10	23	1129±11	35	1816±14	47	1321±12
12	1196±11	24	1237±11	36	1973±14	48	1011±10
						49	1185±11

Table.3.3: Experimental results after exposing the detector unit to ^{60}Co on each cell

Cell #	CPS	Cell #	CPS	Cell #	CPS	Cell #	CPS
1	795±9	13	635±8	25	901±10	37	648±8
2	722±9	14	832±9	26	846±9	38	836±9
3	865±9	15	861±9	27	851±9	39	668±8
4	709±8	16	869±9	28	784±9	40	794±9
5	855±9	17	771±9	29	851±9	41	836±9
6	594±8	18	865±9	30	847±9	42	642±8
7	662±8	19	869±9	31	741±9	43	794±9
8	523±7	20	710±8	32	588±8	44	637±8
9	611±8	21	587±8	33	442±7	45	674±8
10	468±7	22	465±7	34	603±8	46	499±7
11	478±7	23	581±8	35	636±8	47	630±8
12	602±8	24	622±8	36	773±9	48	447±7
						49	498±7

Table.3.4: Experimental results after exposing the detector unit to ^{137}Cs on each cell

Cell #	CPs	Cell #	CPS	Cell #	CPS	Cell #	CPS
1	7333±27	13	5666±24	25	8677±30	37	7757±28
2	6628±26	14	7449±27	26	8011±28	38	8052±28
3	8536±29	15	8522±29	27	8377±29	39	6919±26
4	6875±26	16	8542±29	28	7393±27	40	5904±24
5	8187±29	17	7584±28	29	8087±28	41	7693±28
6	5115±23	18	8356±29	30	8009±28	42	6009±25
7	6043±25	19	8246±29	31	6480±26	43	7638±28
8	4188±21	20	6430±25	32	5483±23	44	5214±23
9	5849±24	21	5697±24	33	4678±22	45	6316±25
10	4309±21	22	4739±22	34	5528±24	46	4563±22
11	5023±22	23	5462±23	35	5776±24	47	5759±24
12	5545±24	24	5622±24	36	7141±27	48	4349±20
						49	4645±21

Table.3.5: Experimental results after exposing the detector unit to ^{36}Cl on each cell

Cell #	CPS	Cell #	CPS	Cell #	CPS	Cell #	CPS
1	11728±34	13	8933±30	25	13968±37	37	12636±36
2	10085±32	14	11665±34	26	13155±36	38	12820±36
3	13846±37	15	13822±37	27	13802±37	39	10551±33
4	10924±33	16	13762±37	28	11956±35	40	8857±30
5	13172±36	17	12360±35	29	13081±36	41	12129±35
6	7592±27	18	13859±37	30	13168±36	42	10321±32
7	9170±30	19	13627±37	31	11294±34	43	11695±34
8	7176±27	20	10384±32	32	8980±30	44	12129±35
9	8896±30	21	8733±28	33	7486±27	45	10321±32
10	7266±27	22	7117±28	34	8794±30	46	7668±28
11	7385±27	23	7509±27	35	9634±31	47	9339±31
12	8478±29	24	9210±30	36	11925±35	48	6558±26
						49	6563±26

3.4. Background Spectra

For the same reason as before, to guide the Monte Carlo Simulation for further improvement, an experiment at a nuclear power plant site has been conducted and Fig.3.5 is the background spectra measured in this experiment to find the most gamma background sources with their activities and energies (see Appendix C). These sources give an input to guide the simulation further.

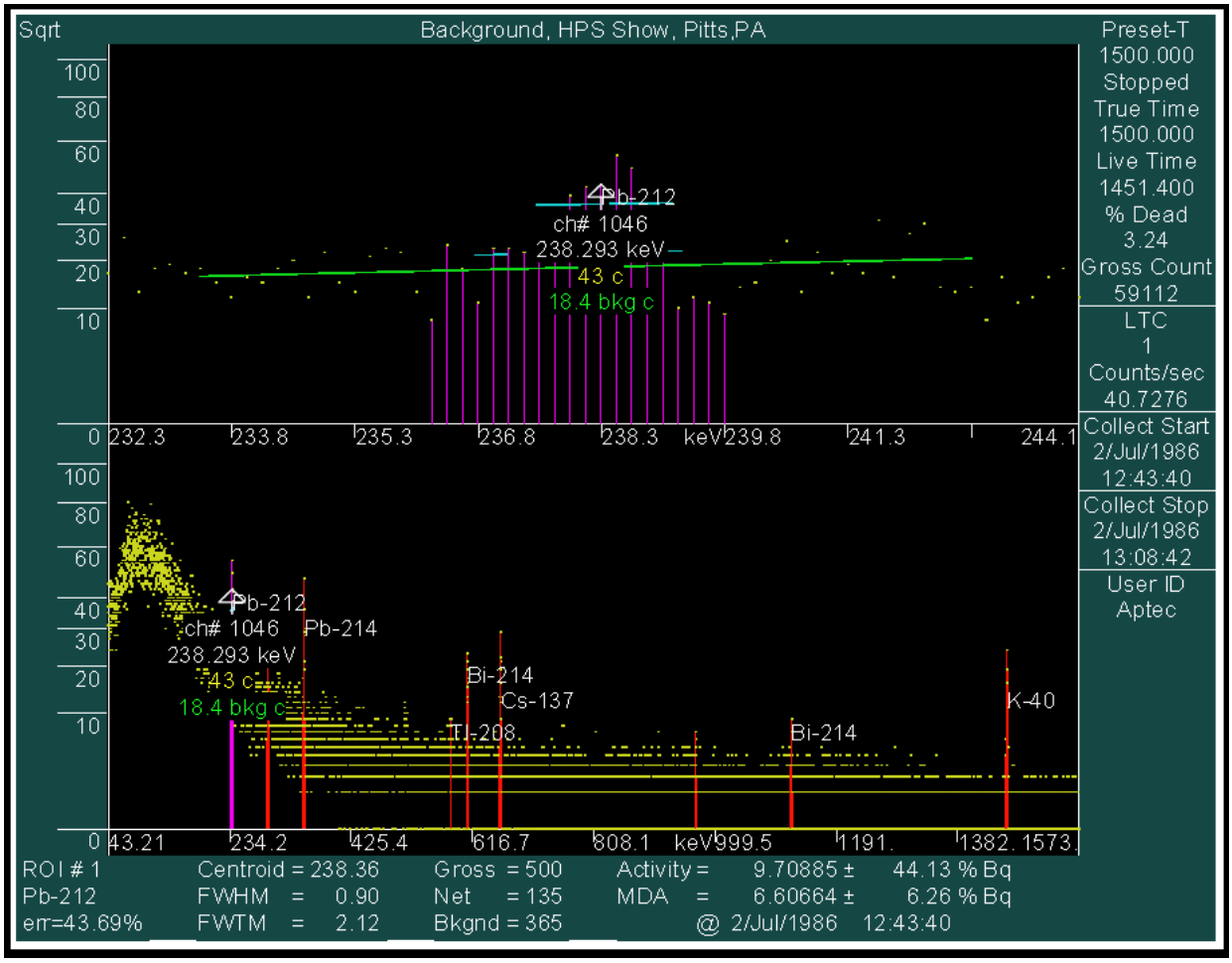

Fig.3.5: Background gamma radiation measured at a nuclear power plant site

Chapter 4: **Monte Carlo Code Description and Simulation**

4.1. Monte Carlo N-Particle Extended (MCNPX) Description

The Monte Carlo method was developed at Los Alamos National Laboratory during the Manhattan Project in the early 1940s. This method is often used to perform radiation transport calculations. MCNP (Monte Carlo N-Particles) is a general-purpose Monte Carlo radiation transport code for modeling the interaction of radiation with different materials. The code can perform coupled neutron-photon-electron transport calculations. Recently, it has been extended to include other particles, physical models and reduction techniques and it gained the name of MCNPX. The last version of the code includes the capabilities to nearly all particles, nearly all energies, and to nearly all applications without an additional computational time penalty. MCNPX is fully three dimensional and time dependent. It utilizes the latest nuclear cross section libraries and uses physics models for particle types and energies where tabular data are not available [15]. It includes application range from outer space (the discovery of water on Mars) to deep underground (where radiation is used to search for oil and gas). MCNPX is used for nuclear medicine, nuclear safeguard, accelerator applications, homeland security, and much more. The code is written in Fortran 90, runs on PC Windows, Linux, and UNIX platforms. As with MCNP, MCNPX uses nuclear data tables to transport neutrons, photons, and electrons. Unlike MCNP, MCNPX also uses (1) nuclear data tables to transport protons; (2) physics models to transport 30 additional particle types (deuterons, tritons, alphas, pions, muons, etc.); and (3) physics models to transport neutrons and protons when no tabular data are available or when the data are above the energy range of 20 -150MeV, where the data tables end [15]. Los Alamos researchers are using it to design detectors that monitor plutonium in nuclear fuel rods, to guide experiments that will test new

nuclear fuels, and as an accurate simulation tool for tracking the physics in next-generation fast reactors. MCNPX is an extremely useful tool for shielding or energy deposition calculations. For detector design, the code is generally used to optimize the design of the detectors before they are built. This saves a lot of experimental work on prototypes [15].

The code treats an arbitrary three-dimensional configuration of materials in geometric cells bounded by first-and second-degree surfaces and fourth-degree elliptical tori. The package also includes cross section measurements, benchmark experiments, deterministic code development, and improvements in transmutation code and library tools [21]. MCNPX calculation has different methods and theory for different particles. Electron transport in MCNP is discussed in Appendix A.

Below are the principal features of the MCNPX version 2.3.0

- Physics for 34 particle types;
- High-energy physics above the giga-electron-volt range;
- Neutron, proton, and photonuclear 150-MeV libraries;
- Photonuclear physics;
- Mesh tallies;
- Radiography tallies;
- Secondary particle production biasing;
- Automatic configuration for compilation.

- (nucleons and light ions) and 2000+ heavy ions at nearly all energies

To write a proper code in MCNPX, there is a structure of input file which consists of several files that are provided as part of the code package, generated by problem runs, or user-

supplied. This section focuses on the user-supplied INP (the default name of the input file) file which describes the problem to be run [15]. In our case we used the code to optimize the thickness of a plastic scintillator to increase the detector efficiency of β particles. These data may be obtained potentially more quickly and economically, by the use of MCNPX modeling techniques before any design.

The MCNP input file or "INP" file contains information about the problem, including the geometry specification; the description of materials and selection of cross-section data used in the calculation; the location and characteristics of the source; the type of output data or "tallies" desired; and any variance-reduction techniques used to improve the efficiency[15]. The structure of an input file, generally, looks as follow:

- Geometry specification
- Materials selection and properties
- The location and characteristics of the source
- Output desired (tallies)
- Any variance reduction techniques used to improve the simulation efficiency

The geometry is constructed by defining cells that are bounced by one or more surfaces. Cells can be filled with a material or be void. Each cell has an importance for each particle type being transported. An importance of zero means the cell is a sink for any particle entering the cell. Every geometry must be completely surrounded by zero importance space (for all particle types) to avoid going "forever process". The material block provides the material definition according to the format required by the cross section generation code. Specification of materials filling the various cells in an MCNPX calculation involves the following elements:

a. Defining a unique material number,

b. The elemental (or isotopic) composition and,

c. The cross section compilations to be used.

Another part of the input file is simply a description of what output is wanted and it is called tally (or tallies). The tally cards are used to specify what type of information the user wants to gain from the MCNPX calculation. There are various types of tallies, like; flux on surface, energy deposition in cells….etc. The source specification „SDEF card' i.e. source definition is the part where the source is defined in the input file is. The SDEF command has many variables or parameters that are used to define all the characteristics of all sources in the problem, and only one SDEF card is allowed in an input file [15].

4.2. Visual Editor

MCNP/X enables a visual creation of an MCNP/X input file which can be read by the Monte Carlo transport code. The Visual Editor was developed to make the creation and debugging of MCNP geometries easier. It is a powerful visualization tool that can be used to rapidly create complex geometry models, including lattices, universes, fills, and other geometrical transformations for use with MCNP/X. The MCNP/X Visual Editor is a graphical user interface for the MCNP/X computer code. The visual editor has powerful display capabilities including the ability to display multiple cross-sectional views of the geometry with optional display of particle tracks during the random walks [24]. The visual editor also includes geometry creation capabilities that allow the user to create MCNP/X geometries directly from the plot window using the mouse. These capabilities provide the MCNP/X programmer with the tools to quickly create complex geometries and display important features of the transport process.

A screen shot of the visual editor is shown in Fig.4.1. The screen in this figure presents the unit that this work has been dedicated to simulate.

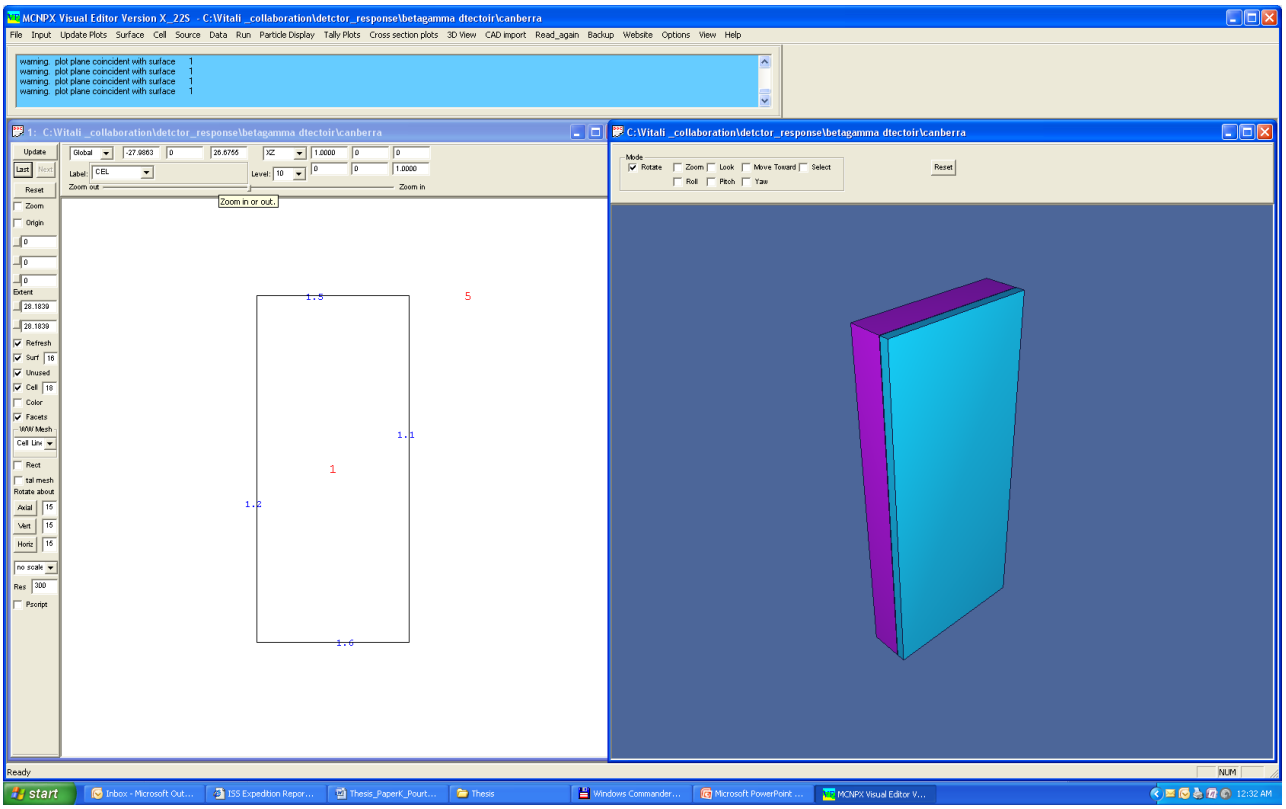

Fig.4.1. A screen shot of the visual editor

The visual editor can:

- Display MCNP geometries in multiple plot windows
- Create surfaces and cells to build geometry
- Create materials using the local xsdir file (data library)
- Store commonly used materials in a material library
- Sub-divided large cells to smaller ones
- Full geometry capabilities including universes and lattices
- Interactively set cell importance from the plot window
- Display source points and collision points in the plot window

4.3. Geometry and characteristics of the detector

4.3.1. Detector geometry

The unit detector tested experimentally in chapter 2 is used in many of CANBERRA monitors and as it will be seen later, with 150μm thickness the unit has low detection efficiency. A number of this unit detector is used in different models monitors in different configuration depending on the task of the monitor and particle to be detected. The unit consists of one plastic scintillator mounted on a plastic box for light collection (light pipe) and it is shown in Fig.4.2. The unit is covered with a reflector for better light collection. To achieve the best performance, the MCNPX simulation model was designed to match the geometry of the unit as faithfully as possible (see details later).

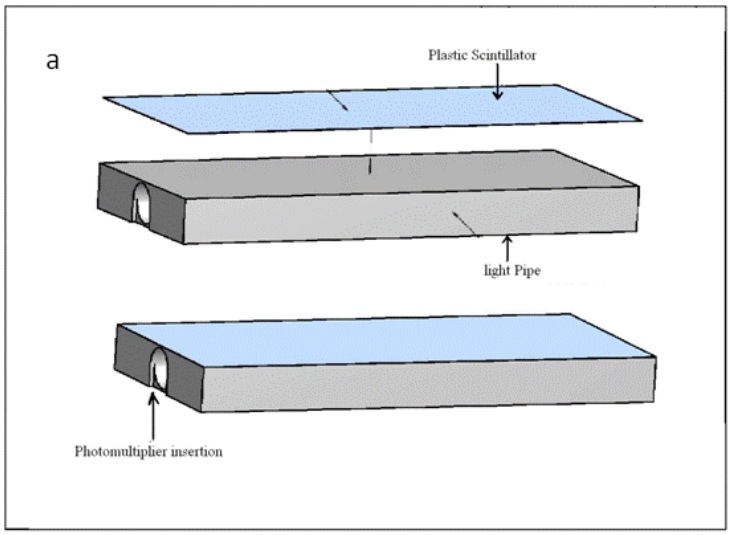

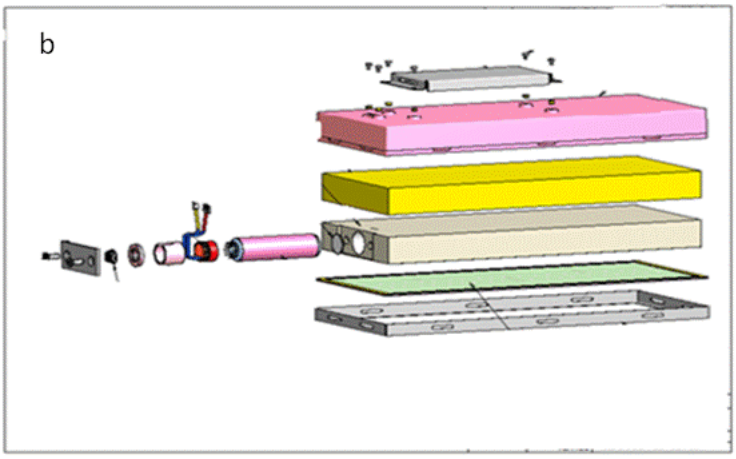

Fig.4.2: (a) Detector unit including thin plastic scintillation layer and plastic box; (b) Detector unit including all component layers, PMT and other protection covers

4.3.2. Detector characteristics

The detector unit is illustrated in Fig.4.3, with all its characteristics and dimensions. Each component is described later in this section.

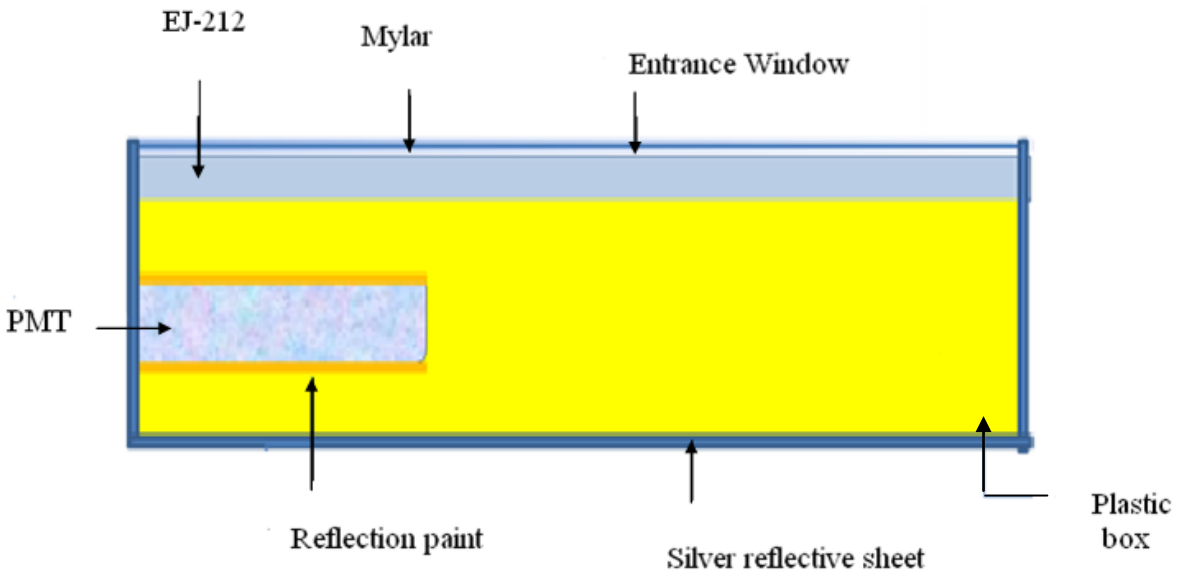

Fig.4.3: Characteristics of the unit used for MCNP model with dimension of 36.05x15.84x3.53cm

a. EJ-212-Scintillation Layer

Fast timing with detectors based on plastic scintillators requires maximum efficiency in the collection of light from the scintillator. EJ-212, or the equivalent BC-400 thin films are ideally suitable for charged particle detection and fast timing applications, they have highest light output and ideal for beta detection [10]. EJ-212 embodies the formula and excellent overall characteristics of the most diversely applied plastic scintillators used over past twenty years. It is stable in water, dilute acids and alkalis, lower alcohols and silicone greases. For more information about the EJ-212 see Appendix E.

b. Plastic box- PMMA Plate EJ-500

Good optical transmission across a broad range of wavelengths and highly polished surfaces to promote total internal reflection is the key performance parameter of a light pipe. PMMA is a versatile polymeric material that is well suited for many imaging and non-imaging microelectronic applications. EJ-500 is clear and colorless epoxy cement with refractive index at 1.57. It is ideal for optically bonding plastic scintillators and acrylic (PMMA) light guides. It is equally effective with PVT (Polyvinyltoluene) or polystyrene based on scintillators. For bonding plastic scintillators, the surface to be joined should by lightly sanded with a 400 grit silicon carbide paper, cleaned with methanol or isopropanol and dried[10].

c. Photomultiplier-PMT

The scintillation layer and plastic box were optically coupled to a single PMT (A cylinder shape with dimension of 14.69 by 3.17cm) with an integrating preamplifier, and then rising pulses from the preamplifier were digitally captured and analyzed by electronics equipments. The PMT was chosen to match the emission spectra of the plastic scintillator EJ-212

d. Entrance Window

It is a comb shape of plastic to protect a Mylar sheet and scintillation layer. Fig.4.4 illustrates the top view of such window.

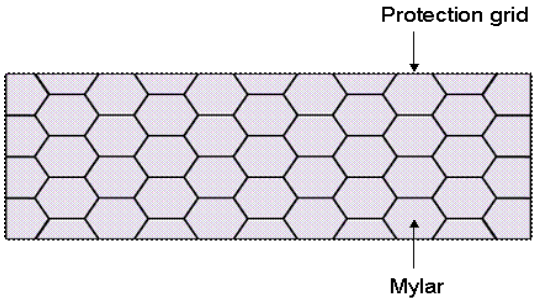

Fig.4.4: Entrance window made of comb shape.

e. Mylar-Polyester film:

It is a Mylar-Polyester film which retains good physical properties over a wide temperature range (-70 to 150^{o}C) with a density of 1.39g/cm^{3}. It is also used at temperatures from -250 to 200^{o}C when the physical requirements are not as demanding [11].

f. TiO2, EJ-510

This is reflective paint for plastics and crystals. It is a bright white paint consisting of titanium dioxide pigment and a water soluble paint base selected for excellent resistance to yellowing and good adhesion [11].

g. Silver reflective sheet

Scintillation light is emitted in all directions and geometrically only a limited fraction can travel directly to the surface of PMT. The remainder must be reflected one or more times at the scintillation surfaces. To recapture the light that does escape from the surface, the

scintillator is surrounded by a reflector at all surfaces except the entrance. Reflectors can be either specular (mirror like) or diffuse (make light spread). In this unit detector, the reflective sheet acts as a specular. It is a Silver reflective film as a hard-coat layer with thickness of $55\mp5\mu m$ and a density of $73x10^{-4}g/cm^2$ which has reflective rate$\simeq$96 %[11].

4.4. Simulation

The existing unit at CANBERRA has a thickness of 150 μm. The goal in this simulation is to determine the optimum thickness of the plastic scintillator to efficiently stop beta radiation and let gamma ray pass through. Schematically, Fig.4.5, illustrates such a situation.

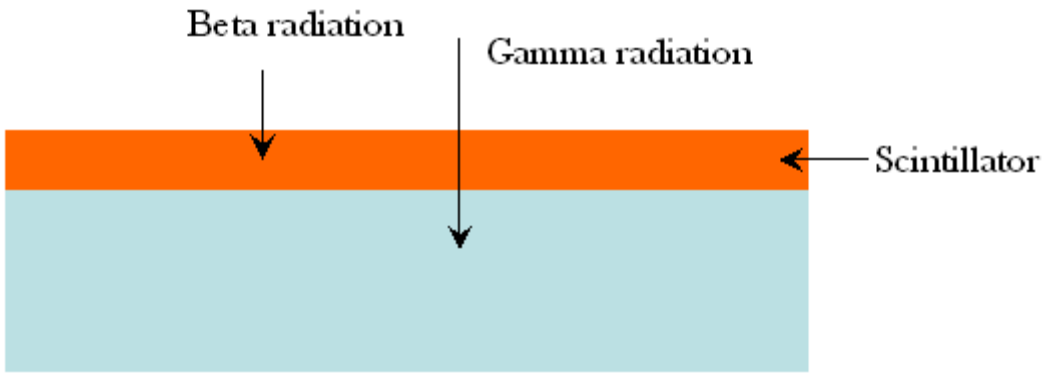

Fig.4.5: Illustration of gamma and beta radiation interaction with the scintillator

The Monte Carlo model was designed and employed to determine the transmission of beta particles and gamma rays through the scintillation material and to match the physical device as faithfully as possible. Prior to the development of the generic methodology shown in this research, it was appropriate to identify the types of models to achieve the highest rate of photons that reach the PMT when beta radiation interacts with the plastic scintillator. At this

stage, using the MCNPX code, we built a simple model of the existing detector unit which matches the exact dimension of the unit. The model consists of calculating the integrated average flux in whole plastic box when the unit is irradiate with beta as well as with gamma and then compared the number of photons for both cases. However this model was very generic and it doesn't help to optimize the position of the PMT in the plastic box. Therefore, a second model has been built and it consists of dividing the unit in 55 cells. Each cell has the same dimension of the entrance widows of the PMT. Furthermore, this model has been used not only for photon counting in different cells but also for calculating the deposited energy in each cell.

4.4.1. The first model

The first model has been built based on 2 boxes, one for scintillating material and the second one for light pipe as shown in Fig.4.6, the same model is shown as a snap shot from the visual editor of MCNPX in Fig.4.7.

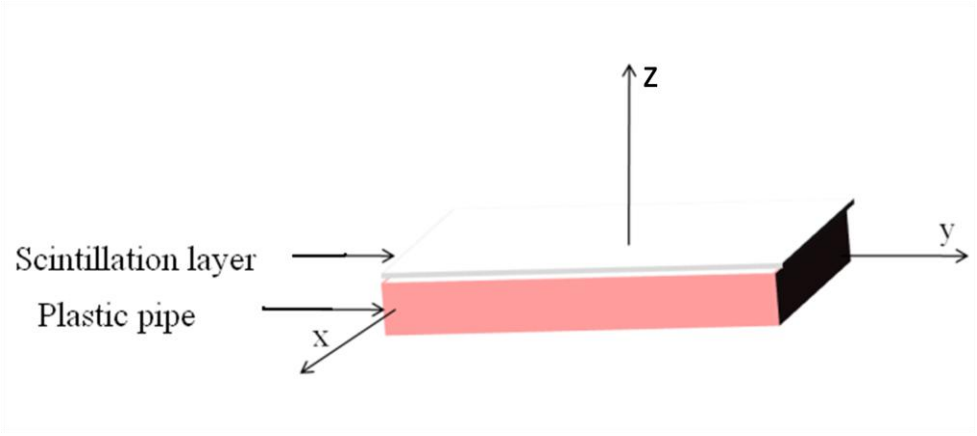

Fig.4.6: First model built in MCNPX

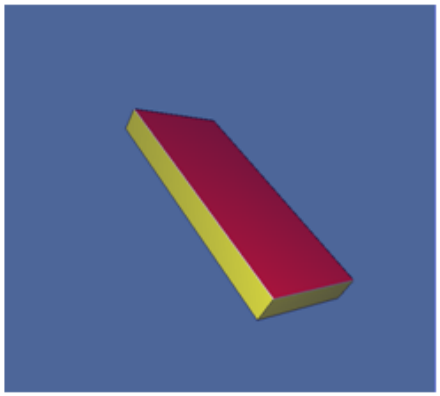

Fig.4.7: First model in MCNPX (screenshot from the Visual editor)

The rectangular detector was modeled using the known dimensions and materials of the existing unit detector. The primary item of interest in this model was to count the number of photons in plastic box as a function of the thickness of scintillation layer. However and since MCNP code does not allow to count very low energy photons emitted by the scintillator as a result of interaction with external radiation, we have counted the number of gamma, with energy higher than the cut off, in the light pipe. The photons that result from the beta interaction with the scintillator are below the cutoff and therefore we were not able to count them. Instead we counted the number of electrons that pass though. The plastic scintillator mounted on the guide pipe has been irradiated with different gamma and beta sources that mostly present a concern at workplace.

The result for different thicknesses with low gamma energy of ^{241}Am of 60keV shows that there is a dependence on the thickness of the scintillator. By increasing the thicknesses there is a clear decrease of the number of photons in the plastic pipe caused by stopping more photons in scintillation layer.

The methodology we have adopted is: firstly we track the lowest gamma energy, (^{241}Am, 60 keV) Fig. 4.8. Furthermore, other gamma radiation sources with higher energy have been

simulated. The calculations have been carried out for different thickness from 150 to 600 μm and the number of photons in the guide pipe has been counted.

For low beta energies, the thickness does not contribute that much in the number of photons created, but for high energies the number of created photons increases with the thickness. The energies used were 156KeV, 334KeV, 514KeV, 709KeV.

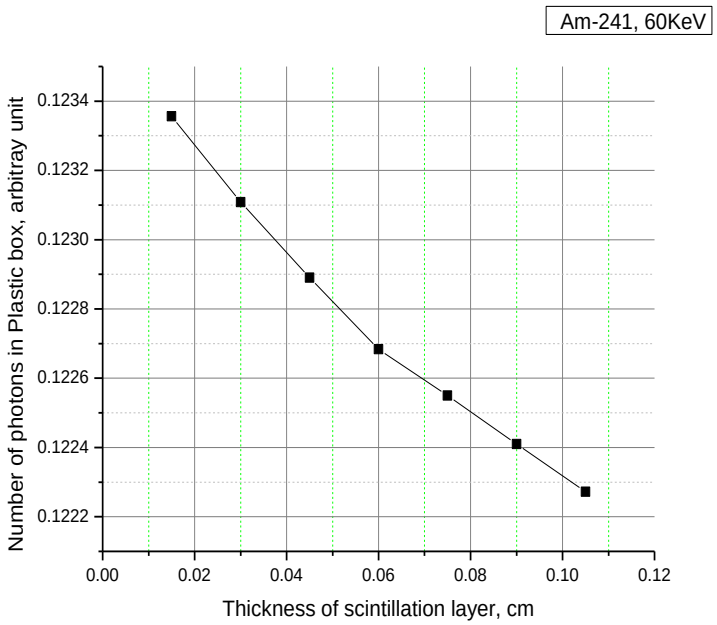

Fig.4.8: Number of photons counted in plastic box for gamma source.

Since the counting efficiency depends not only on the thickness of the scintillation layer but also on the position of the photomultiplier in the light pipe, the other part of the simulation was to find the best position to fix the PMT in the light pipe in order to maximize the light collection and have better efficiency in counting the number photons. For such purpose, the second model has been built where the unit was divided to 55 different cells that have the same size of the entrance windows of the photomultiplier. The methodology was as follows:

Since the diameter of PMT is 3.17 cm, the second model has been built in such a way that the size of the each cell coincides with the dimension of the PMT entrance window i.e. 3.17cm in diameter. Therefore, the plastic box where the PMT reside was divided to 55 cubic cells of 3.3cm in side. The model is described in the next section. The same methodology has been followed for beta radiation, only in this case we count the number of electrons in both layers i.e. the number of electrons stopped in the plastic layer as well as in the guide pipe.

4.4.2. The 55 cells model

To refine the first model and count the number of photons in specific cell, the plastic box was divided in 55 cells (dimension of each cell; 3.3cm by 3.17cm) to match the size of PMT. Fig.4.9, schematically, illustrates such model. The same model as a snap shot from the MCNP visual editor is shown in Fig.4.10. The MCNPX code has been ran in mode e (electrons only), mode p (photon only), and mode e p (electrons and photons). However, since the MCNPX does not simulate low energy photons, only the number of photons higher than the cut off energy was counted.

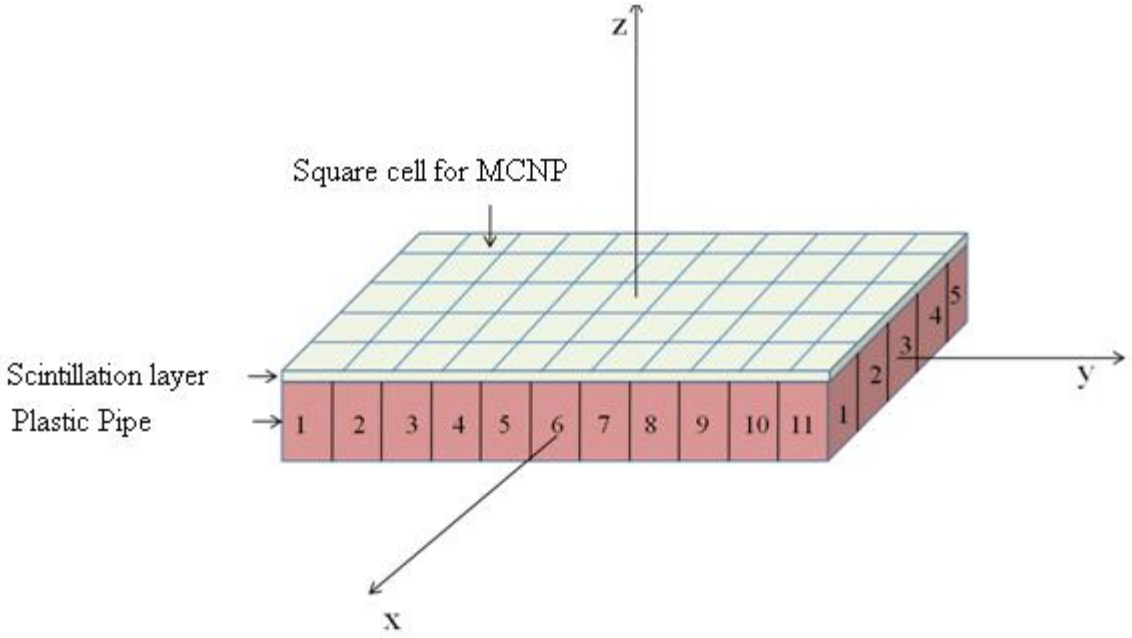

Fig.4.9: 55 cells model to match the size of the PMT

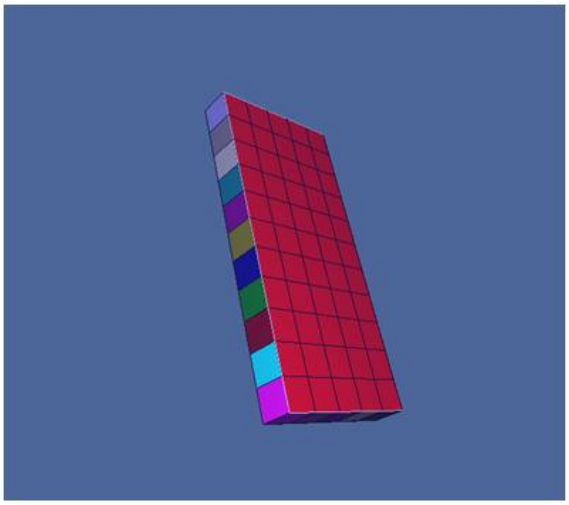

Fig.4.10: 55 cell Snap shot from MCNPX Visual Editor

To quantify the number of photons and electrons in each cell of the plastic box after the interaction of beta-particles and gamma radiation, we calculate the number of electrons and photons that pass through the scintillate layer. One run of this model with a 150μm thickness is presented in Fig.4.11 when the detector has been irradiated with ^{241}Am (60keV) source. The

x-axis in this figure presents the position of each cell of the detector. It is clear that, the cell number 25 which presents the closest cell to the entrance widow of the PMT has the largest number of photons (see Fig.4.9).

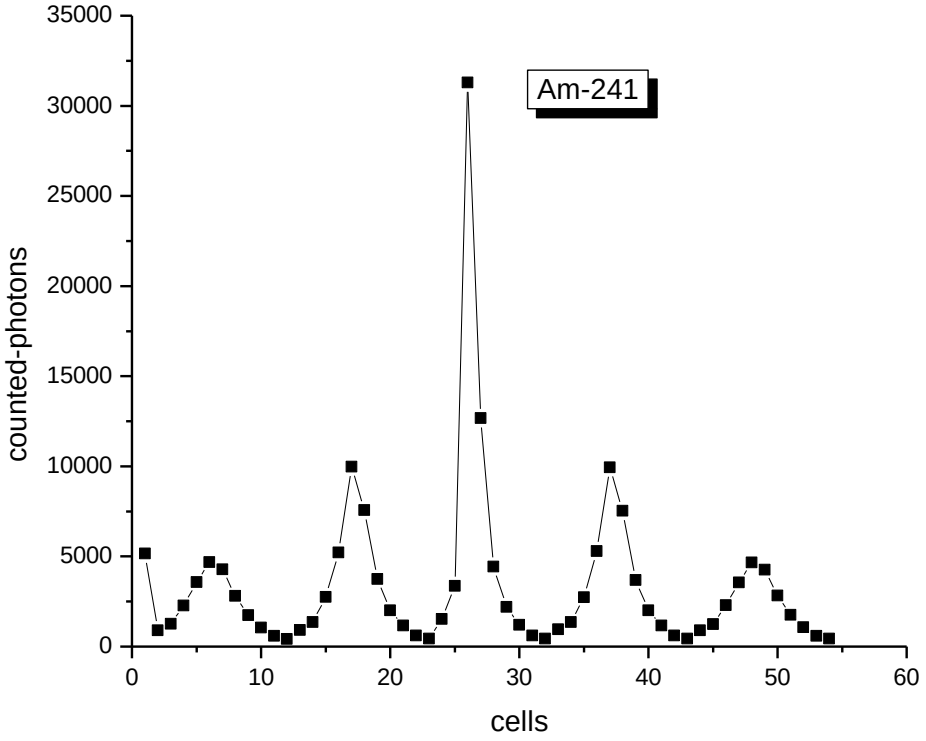

Fig.4.11. Counted-photons in different cells in the second model by putting ^{241}Am on each cell for the detector-unit with 150μm thickness (see Fig.4.9 for cell coordinates).

The same calculation has been performed for electrons. For instance, a ^{60}Co source with 0.344 MeV has been located on different cells, then the number of electrons in cell 25 has been counted and the obtained results are shown in Fig.4.12. Again it is clear that the largest number of electrons is accumulated in cell 26. Probably, this is due to multi scattering process

as well as to the scattered electrons generated by the Compton scattering of the gamma radiation.

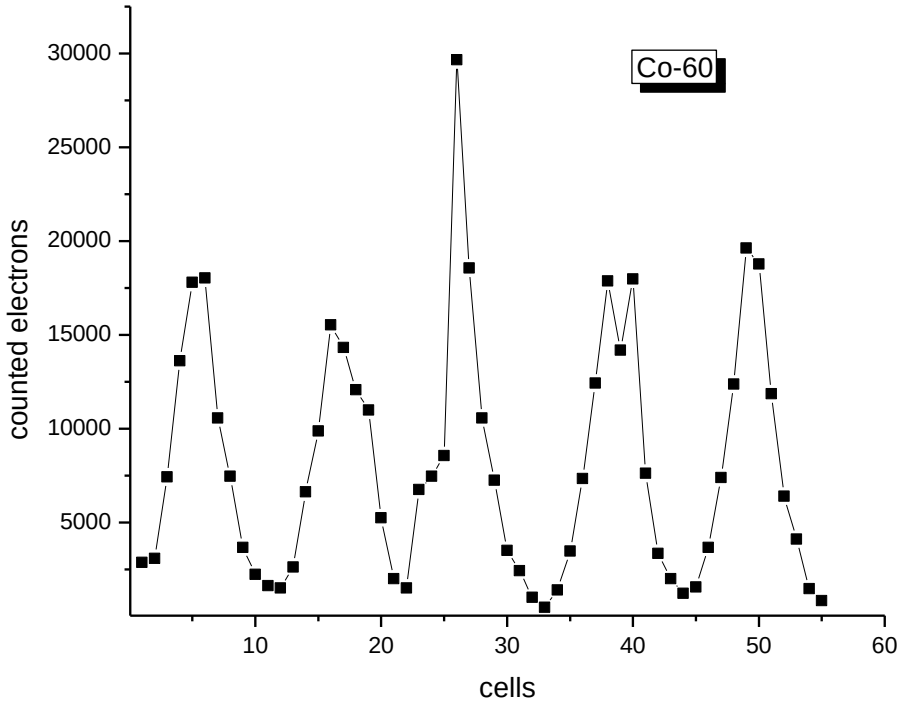

Fig.4.12: Number of electrons in plastic box generated by locating ^{60}C0 on each cell for the 55-model (see Fig.4.9 for cell coordinates)

In the next step, the same methodology has been followed to check the influence of the thickness on the number of photons in each cell. The obtained results are illustrated in Fig.4.13.

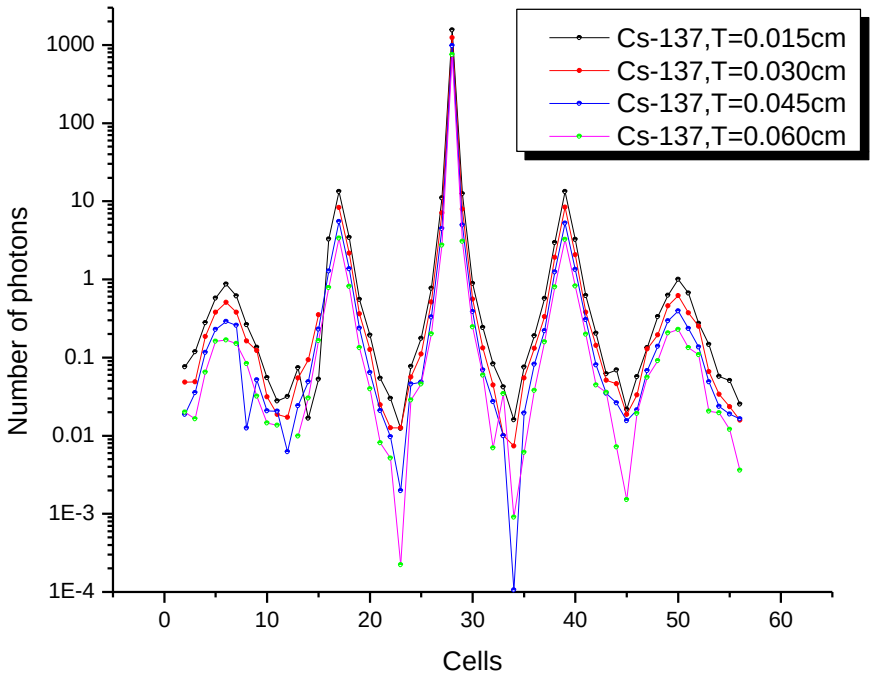

Fig.4.13: Comparison between numbers of photons in different cells through different thicknesses for ^{137}Cs

4.4.3. Deposited energy model

The number of photons calculated in the entire plastic box (first model) or in a single cell didn't help to make a decision regarding the optimization of the thickness of the scintillation layer, more precisely, the right thickness that stops efficiently beta radiation with the maximum energy possible and allow gamma radiation with the minimum energy possible to pass through. After long discussions in different meetings and consultation with experts in MCNPX, we come out with the last model that uses a fundamental physics principle of energy deposition.

Since the number of photons created in the plastic scintillator depends on the number of excited molecules which itself depends on the incoming particles and the thickness of the

scintillation layer, it is indispensible to use the deposited energy as fundamental criteria to optimize the layer thickness. Such approach has been adopted in the last model of the optimization. Thus, a model has been build based on calculating the deposited energy in scintillation layer for different thicknesses for beta as well as for gamma with different energies. We have used the feature of one of the eight tallies of MCNPX, namely the F8 tally that records the electron and photon energy deposition in each plastic cell and we ran the code in different modes:

1. gamma source only
2. beta radiation only
3. mixed field of beta and gamma

4.4.3.1. Gamma deposition

As a starting point, we have used 150 μm thickness and we have calculated the deposited energy in the scintillation layer. The results of such calculation are shown in Fig.4.14 for different gamma energies. There is a clear increase in the energy deposition for low gamma energy radiation. But for higher gamma energies, the resulting electrons from the photon interaction with the plastic scintillator travel faster and the energy deposition decreases.

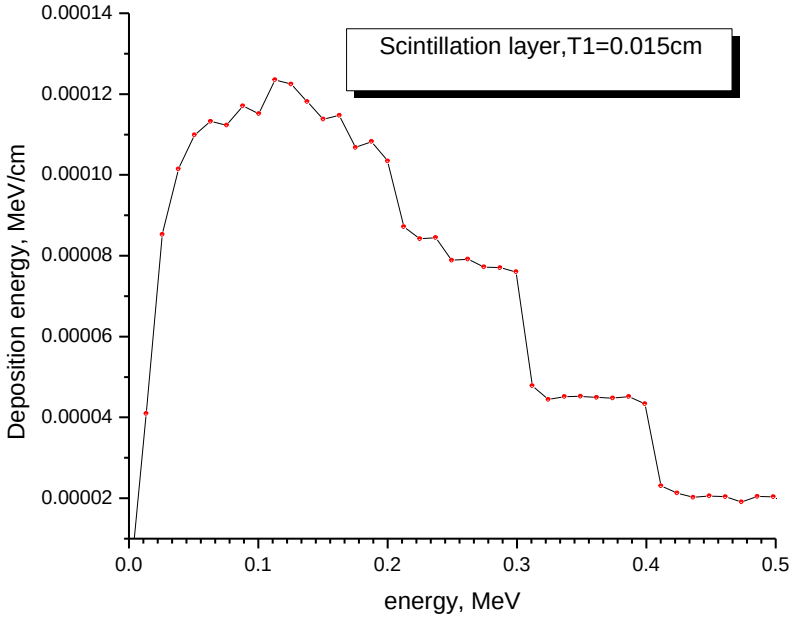

Fig.4.14: Deposition energy in scintillation layer for gamma-radiation in existing detector unit

Moreover, in Fig.4.15, we derived this investigation a bit further by increasing the thickness of the scintillation layer and did the same simulation for greater thicknesses.

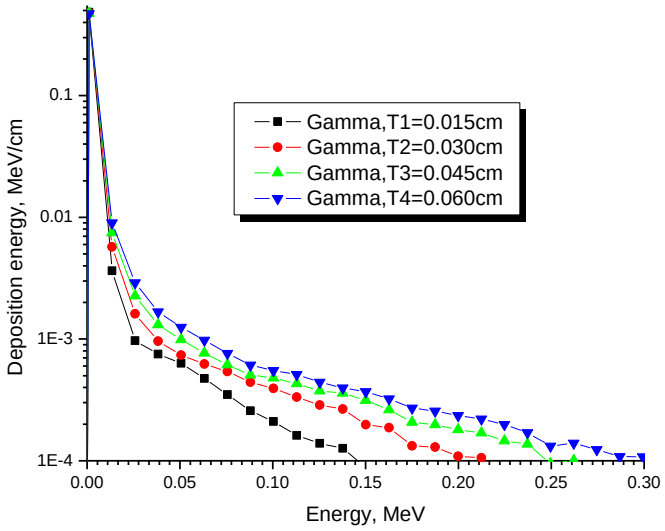

Fig.4.15: Deposition energy in scintillation as a function of gamma and thickness of the scintillation layer

4.4.3.2. Beta simulation

The same methodology has been used for beta radiation and the unit has been irradiated with different beta energies. Fig.4.16 shows the obtained data for two thicknesses of 150 and 300 μm. For other thicknesses, the results are shown in Fig.4.17.

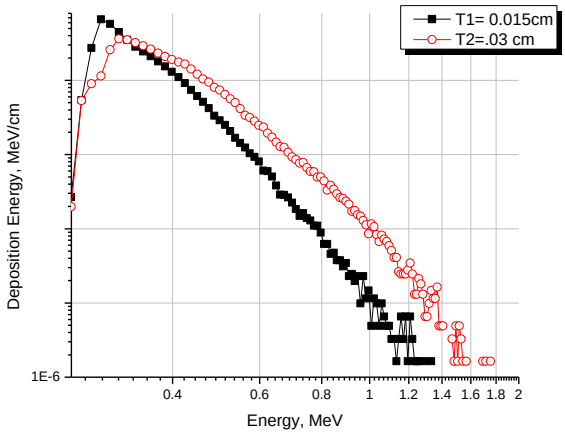

Fig.4.16: Beta deposited energy in scintillation layer for two thicknesses

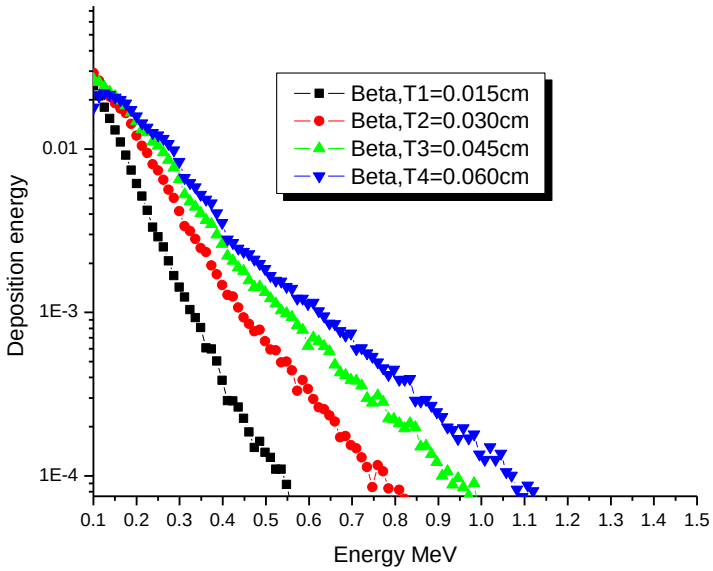

Fig.4.17: Comparison of Beta deposited energy in scintillation layer for different thicknesses

At a fixed thickness the deposited energy for different beta sources is illustrated in Fig.4.18. The analysis of this data will be discussed later in chapter 5.

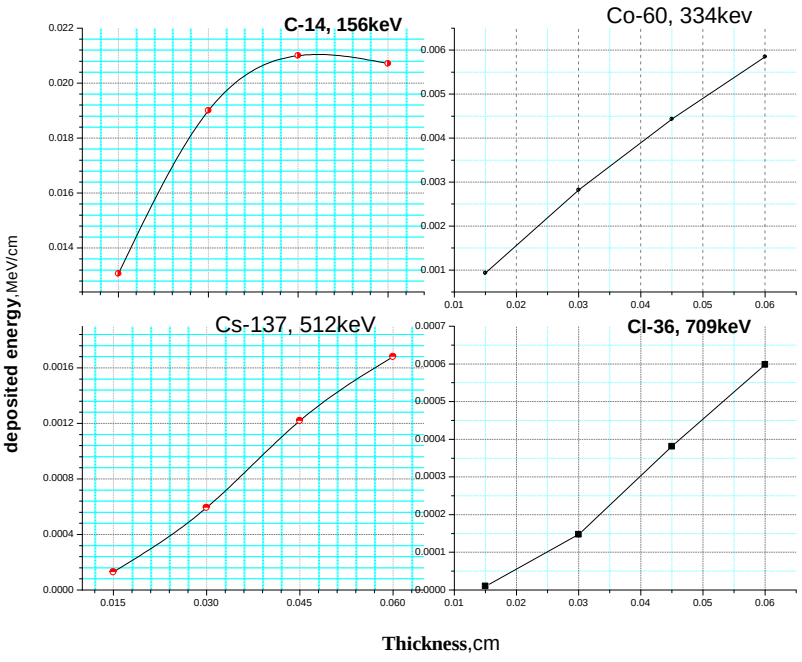

Fig.4.18: Deposited energy for different beta sources

The calculation performed with beta has been compared to gamma radiation and the results are shown in Fig.4.19 when the unit was irradiated by different gamma and beta sources for different thicknesses.

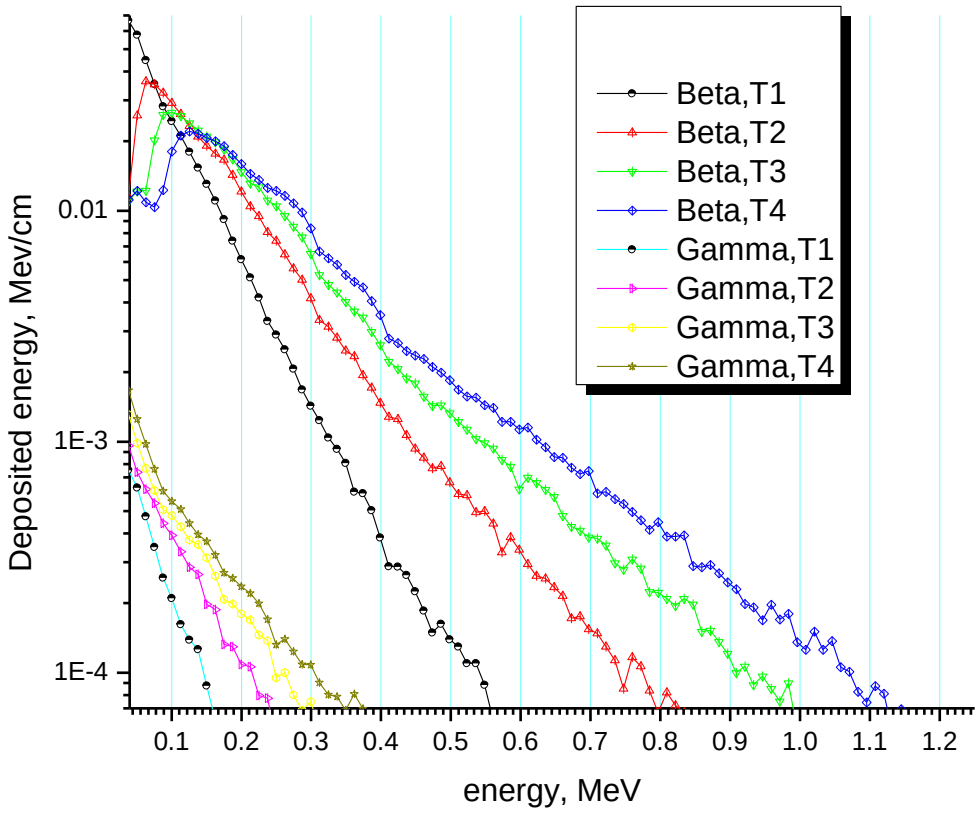

Fig.4.19: Difference in deposition energy for beta and gamma radiation as a function of scintillation layer thickness

Chapter 5: Analysis and Discussion

The purpose of this chapter is to analyze the results obtained in the experimental test in chapter 3 and link the findings to MCNPX results in chapter 4.

5.1. Experimental data analysis and discussion

To analyze the performance of the detector, the experimental data (Table 3.2 to 3.5) measured with different beta sources placed on the top of the scintillation layer at different positions were converted to 3 dimension graphs for each experiment. Knowing the activity of the source, the efficiency of the detector has been measured. For the measurement with ^{14}C (156 keV), Figure 5.2 shows the variation of the photon number as a function of the position on the x- and y axis. The road map (coordinates) of each cell is shown in Fig.5.1. The measurements have been carried out with other beta sources namely, ^{60}Co, ^{137}Cs and ^{36}Cl. The experimental data are shown in Fig.5.3 to Fig.5.5, respectively.

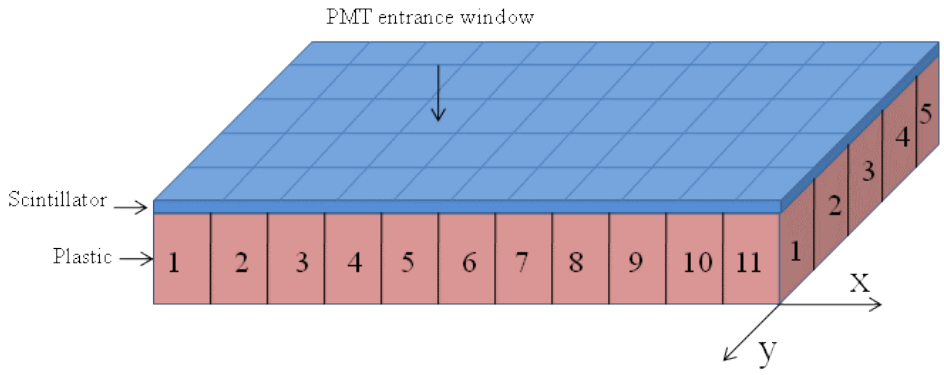

Fig.5.1. Roadmap of different positions relatively to the PMT

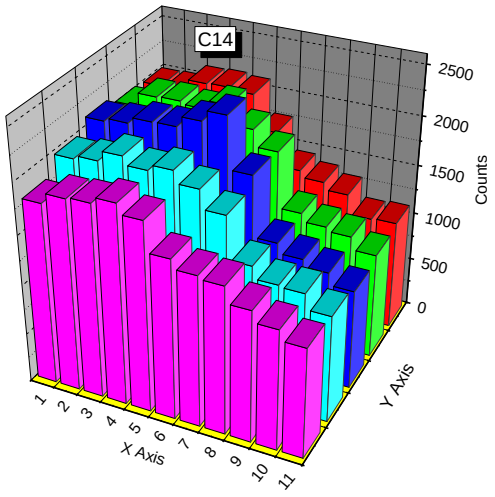

Fig.5.2. Measurement of counted-photons when the unit was irradiated with ^{14}C on different cells

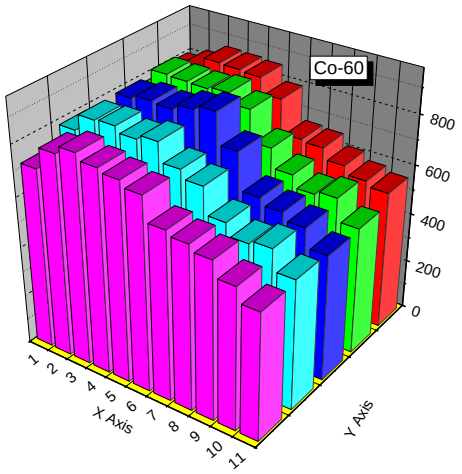

Fig.5.3: Measurement of counted-photons when the unit was irradiated with ^{60}Co on different cells

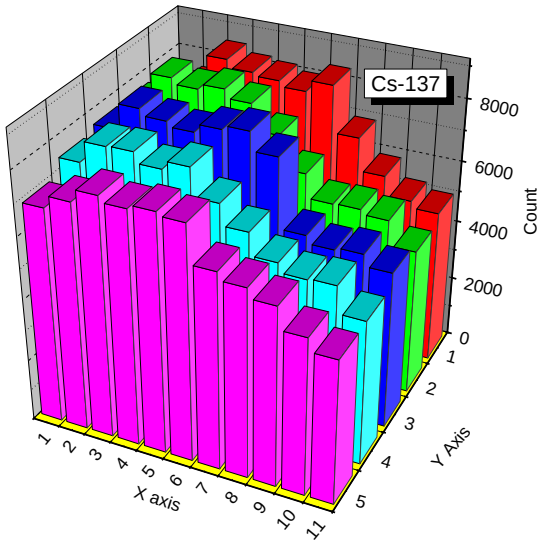

Fig.5.4: Measurement of counted-photons when the unit was irradiated with ^{137}Cs on different cells

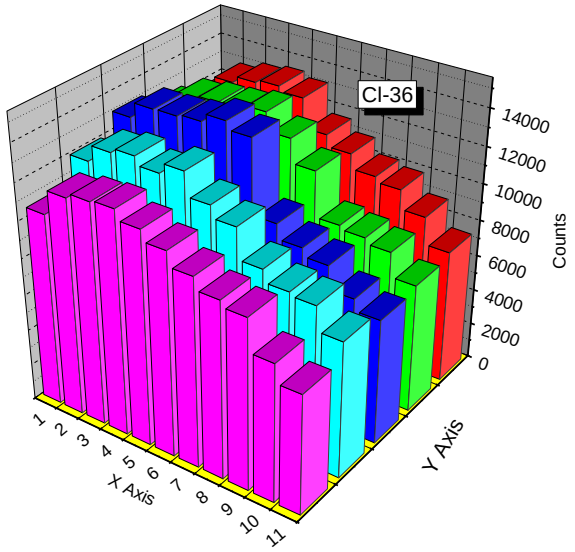

Fig.5.5: Measurement of counted-photons when the unit was irradiated with ^{36}Cl on different cells

It is clear that as the beta energy increases from 156 to 709 keV, at the entrance windows of the PMT, the number of photons emitted from the scintillation layer increases accordingly and Fig.5.6 shows the behavior of the photons counted when the source is at the closest position to the PMT.

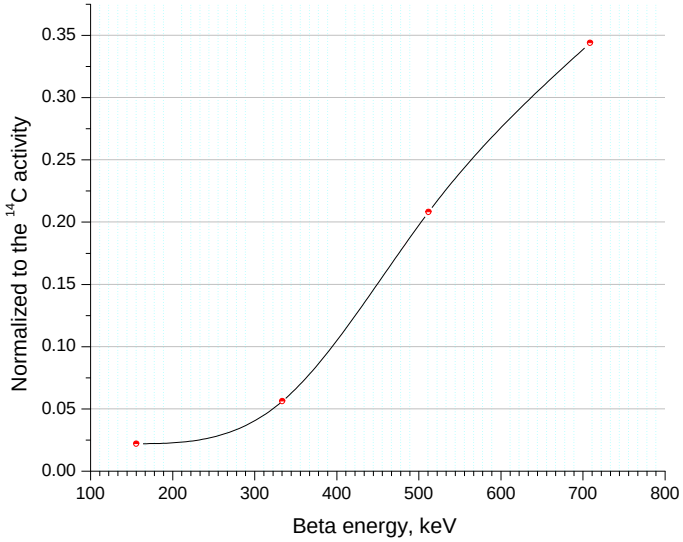

Fig.5.6: Normalized Number of count as a function of the Beta energy

The variation is not linear because of the non linearity of the light output of the plastic scintillator. From the previous figures (Fig.5.2 to Fig.5.5) and depending on the location where the beta particle hit the scintillator, a large portion of emitted photons are guided toward the PMT after reflection against the wall of the detector. All figures are showing a similar behavior and they differ only by the intensity. More explicitly, one can see that the number of photons is almost constant when moving the source along the Y axis at a fixed position on the X-axis. The problem here is purely geometrical i.e. the PMT sees the same number of photons in the solid angle viewing the extremities of the scintillator. By getting

closer to the photomultiplier the solid angle gets wider and the number of photons increases(i.e. moving from cell 11 to cell 1 on Y axis), the efficiency of the detector increases to reach a maximum value at cell 4 where the entrance window of the PMT is located. While when the source is behind the PMT, after cell 5 (Y axis), the efficiency starts slightly decreasing toward cell 1. This decrease is due to the dead zone of the scintillator at the back of the photomultiplier. Fig.5.8 illustrates, schematically, the situation with different solid angles referred to as 1, 2, 3 and 3 in Fig.5.8.

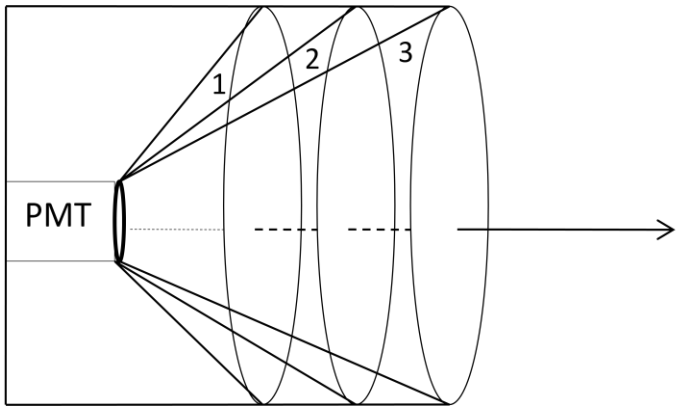

Fig.5.8: Geometrical illustration of the influence of the solid angle on the detection efficiency

It should be mentioned that, the curves are not symmetric and this is expected because of the PMT length is only 5 cm and it does not extended to the center of the detector. The picture can be seen differently in term of distance from the PMT entrance windows: the further the source is from the entrance window, the lesser the number of counted photons is.

The efficiency of the detector has been extracted from the measured data and it presented in Fig.5.8. The ^{14}C beta particle, with the energy of 156keV has the lowest efficiency of around 6%. If we compare this value with the simulation data of the deposited energy we find out that these beta particles deposit the largest amount of energy compared to higher energy beta from ^{36}Cl or other used isotopes in the experiments (^{60}Co and ^{137}Cs). This phenomenon is

understandable since the energy required to excite all molecules at a definite point is limited (saturation, see Fig.2.7) and any extra amount of energy deposited will not increase the number of exited states because after reaching the saturation state, delivering more energy to the material would not increase the light output. This was proved also by the MCNP calculation in Fig.4.18 where a comparison between different beta emitters is given.

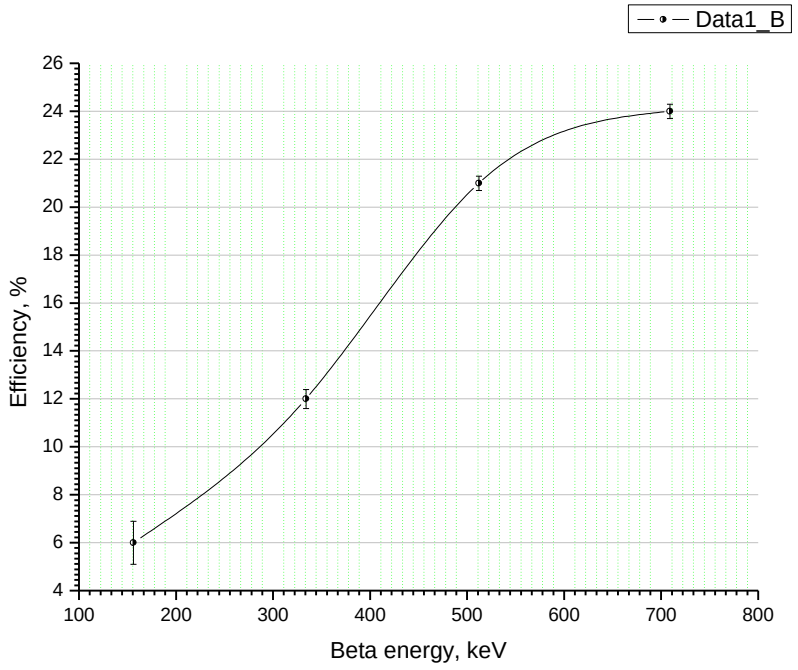

Fig.5.9: Efficiency of the detector as a function of Beta energy

5.2. Simulation data analysis and discussion

As mentioned before, on the light of the experimental data measured with 150 μm, we have used the simulation approach to improve the efficiency of the detector by increasing the thickness of the scintillator. The goal is to find an optimum thickness to stop beta particles and leave the gamma radiation passing though. Fig.5.10. shows the results of the calculation when the thickness of the scintillator has been doubled. For beta energy higher than 100 keV, one

can, clearly, see that the deposited energy increases. For example, this increase is about 20% for energy around 500 keV (marked with two open circles on Fig.5.10). For lower energies the difference is not that remarkable.

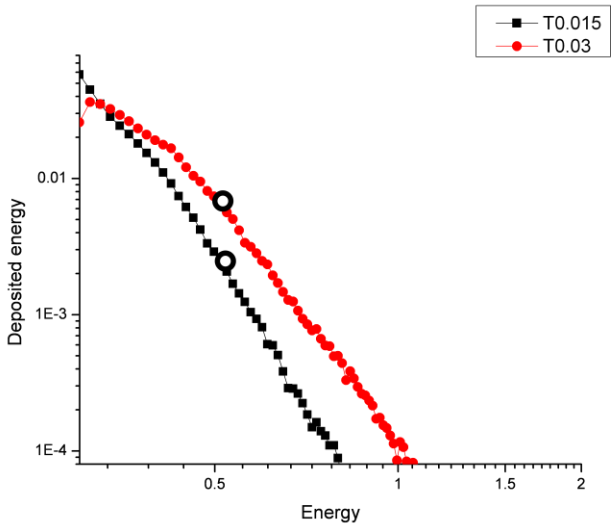

Fig.5.10: Energy deposition for 150 and 300μm thicknesses

For further investigation, we have increased the thickness up to 600 μm by an increment of 150 μm, the results of the simulation are shown in Fig.5.11.

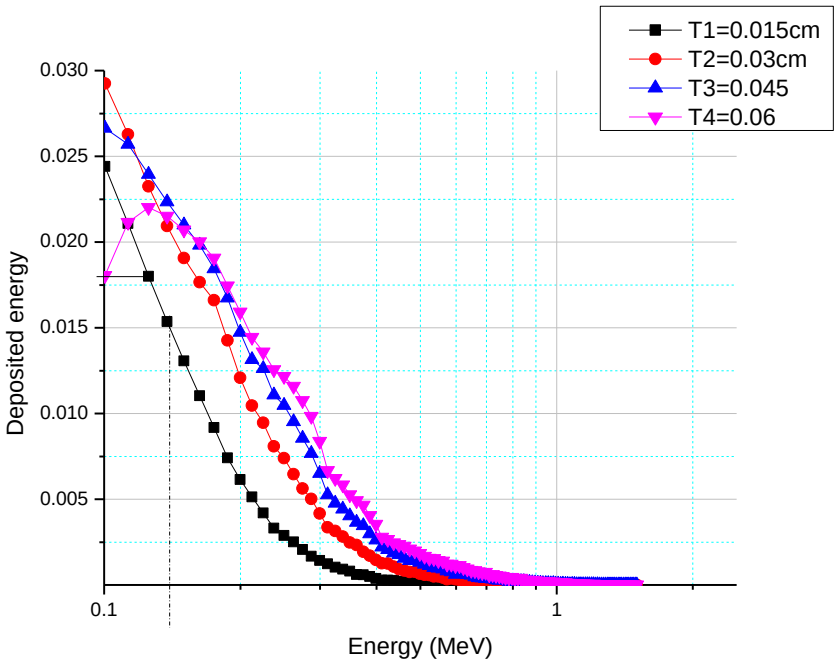

Fig.5.11: Energy deposition as a function of beta energy for different thicknesses

One important feature in Fig.5.11 is that the deposited energy increases slowly almost for all energies and at some point, 450 μm, the thickness does not have that much to add in terms of light output since the number of excited states reaches its maximum value (saturation).

Furthermore, the ratio has been calculated, as a function of the thickness, of the amount of energy deposited in the scintillation layer and in the plastic box (light pipe), the results are shown in Fig.5.12. For ^{14}C, 156 keV, the ratio slightly increases with the thickness up to about 450 μm and reaches the saturation, while for other higher beta energies the increase is remarkable and it presents 16, 14 and 110 times for ^{60}Co, ^{137}Cs and ^{36}Cl, respectively, when compared to only 15% of ^{14}C (when going from 150 to 600μm thickness).

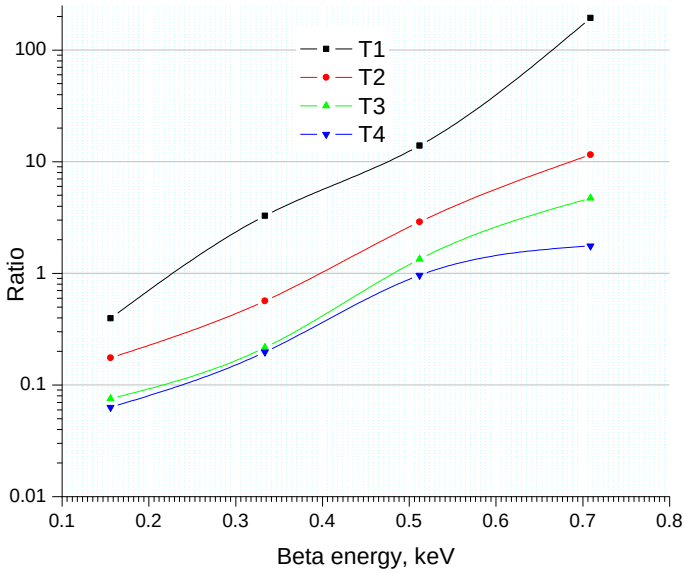

Fig. 5.12. Ratio of deposited energy in plastic box to scintillation layer as a function of thickness and beta particle energy

If linking this to the deposited energy in Fig.5.11, we can conclude that a thickness between 300 to 450μm, will improve the detection efficiency for beta particles. However, to make a final decision for an optimum choice of the thickness, one has to consider how this thickness will influence the gamma contribution to the amount of energy deposited in both layers. To do so, the detector was irradiated with beta particles of ^{14}C and with a low energy gamma source of ^{241}Am and we have calculated the ratio of the deposited energy of gamma and beta. The results of such calculation are shown in Table 5.1.

In Table 5.1, the comparison between ^{14}C (156keV) beta and low energy gamma emitted from ^{241}Am (keV) shows a difference of only 3.2% and 3.6% when we double and triple the thickness, respectively. For any gamma energy higher than 330 keV, which is the case in

those places where this type of monitors is installed, the deposited energy is negligible even for the thickness of 600 μm (4 times thickness).

Table5.1: Ratio of deposited energy of lowest gamma-particle over lowest beta-particle

Thickness, cm	**D_1 = Deposited energy, MeV/cm Am, 60keV**	**D_2=Deposited energy, MeV/cm C14, 156 keV**	**D_1/D_2**
300μm	$6.22*10^{-4}$	$190.0*10^{-4}$	3.2%
450μm	$7.66*10^{-4}$	$210.0*10^{-4}$	3.6%

Conclusion

The characteristic and features of the methods and techniques employed for detecting beta-particles in mixed fields of beta/gamma radiation using thin plastic scintillators has been described. Firstly, an experimental study of a cell unit of Argos-PB contamination monitors model has been conducted to determine the efficiency of the monitor with the existing cell unit of 150 μm thickness using EJ212 plastic scintillator.

The experimental data has shown that the monitor has a low detection efficiency of about 6% for ^{14}C beta emitter and about 24% for ^{36}Cl. Further investigation has been conducted to improve the beta detection efficiency using Monte Carlo Calculation.

The study has been done for different beta and gamma energies with different thicknesses from150 to 600μm to optimize the thickness of the scintillation layer for better beta detection efficiency with a minimum interference of gamma radiation. The deposited energy in the media of the detector has been calculated and the main findings are:

- The deposited energy of beta particle increases by increasing the thickness of the scintillation layer only if the energy of the particle is higher than threshold energy of around 100 keV.
- For any gamma energy higher than 300 keV the deposited energy is negligible.
- The deposited energy in scintillation layer for 60keV gamma presents only 3.2% for 300 μm thickness and 3.6% for 450 μm when compared to 156 keV beta-particles.

- It is expected that for other high energy beta, the percentage ratio of the deposited energy will increase and some more refining calculations should be done.
- A thickness of 300 μm to 500 μm is an optimum thickness for high efficiency beta detection in the presence of low energy gamma ray.

Future work

In view of future developments in this field, a deeper knowledge of the energy transfer processes involved in the light emission mechanisms of thin organic scintillators is required in order to improve the capabilities of the existing system and to give a quantitative evaluation method of the properties of scintillating plastic materials, and better design for light pipes.

Since the unit has been tested only for 150 μm, the next step is to measure the efficiency with at least two other thicknesses namely 300 and 450 μm to refine the MCNP calculations.

The most important direction to move forward is to use a double scintillator detector with different thicknesses to develop a dual unit for dual beta and gamma detection at the same time. Thus, it is planned to change the plastic box to scintillating material to detect gamma-radiation by using coincidence technique.

Finally, the dead zone of the unit been tested is very large and for the best geometry optimization, it is better to use either a short PMT or use more than one in both extremity of the unit. Of course this will go at the expenses of the cost of the monitor.

References

1. Mohamed M. El Baradei, Warner Burkart and Michael F.L'Annunziata. Handbook of Radioactivity Analysis(Second Edition), ISBN: 978-0-12- 436603-9 , 1985
2. James E. Turner, Atoms Radiation and radiation Protection, Third edition, 2007
3. Herman Cember, Introduction to Health Physics,fourth edition, 2008
4. W.R.Leo. Techniques for Nuclear and Particle Physics Experiments, Second Revised Edition, second edition, 1993.
5. Glen F. Knoll, Radiation Detection and Measurement, edition 5, 1989
6. Geoffrey G.Eichholz , John W.Poston. Principles of Nuclear Radiation Detection ,1985
7. Nicholas Tsoulfanidis, Measurement and Detection of Radiation, 1995
8. Claude Leroy, Pier- Giorgio Rancoita, Principal of Radiation Interaction in Matter and Detection, 2004
9. M.S. Dias, H. Piuvezam-Filho, M.F. Koskinas Optimization of a coincidence system using plastic scintillators in 4π geometry, Applied Radiation and Isotopes, Volume 66, Issues 6-7, June-July 2008, Pages 905-908.
10. SAINT-GOBAIN, Organic Scintillation Products, 17900 Great Lakes Parkway Hiram, OH 44234 www.detectors.saint-gobain.com, ELJEN TECHNOLOGY, Sweetwater TX 79556 USA www.eljentechnology.com
11. Canberra Company, Measurement Solution for Nuclear Safety and Security, www.canberra.com
12. http://www.iaea.org/Publications/Magazines/Bulletin/Bull234/23405043136.pdf (Swinth and Sisk, 1991, ICRU 56, 1997)
13. Los Alamos Science and Technology Magazine,MAY 2008, http://www.lanl.gov/news/index.php/fuseaction/1663.article/d/20085/id/13280)
14. Scintillation Mechanism and Efficiency of Ternary Scintillator Thin Films, A. Quaranta, A. Vomiero, and G. Della Mea , IEEE TRANSACTIONS ON NUCLEAR SCIENCE, VOL. 49, NO. 5, OCTOBER 2002
15. Denise B. Pelowitz, MCNPX^{TM} USER'S MANUAL, Version 2.6.0, April 2008
16. H. H. Vo, S. Kanamaru, C. Marquet, H. Nakamura, M. Nomachi, F. Piquemal, J. S. Ricol, Y. Sugaya, and K. Yasuda, Energy Resolution of Plastic Scintillation Detector for Beta Rays, IEEE TRANSACTION ON NUCLEAR SCIENCE, VOL. 55, NO. 6, DECEMBER 2008
17. Sanjoy Mukhopadhyaya, Plastic gamma sensors: an application in detection of radioisotopes, Bechtel Nevada, P.O. Box 98521-8521, M/S RSL-11 Las Vegas, NV 89193-8521
18. Gillespie C.R., Uniformity of Response from large area plastic scintillation detectors, Department of Physics and Astronomy, Louisiana, State University, Baton Rouge, Louisiana 70803. Review of Scientific Instrument, Issue 11,June 2009
19. D.M Hamby and A.T. Farsoni, A System for Simultaneous Beta and Gamma Spectroscopy and its Application to Nuclear Non-Proliferation. Nuclear Engineering and Radiation Health Physics, College of Engineering, Oregon State University,
20. Yu, A, Tsirlin, T. I. Sokolovoskaya, R, A, Nikulina, and L, L. Nagornaya Zhurnal Prikladnoi, Light Yield of Plastic Scintillators in Relation to the Energy of External Electrons, Vol, 3, No. 8, pp. 156-161.
21. H. Grady Hughes, Treating Electron Transport in MCNP, 1997.
22. Nagarkar V. V, Miller SR, Tipnis SV, Lempicki A, Brecher C, Lingertat H A new large area scintillator screen for X-ray imaging**,** 2004 Nuclear Instruments &

Methods in Physics Research, Section B (Beam Interactions with Materials and Atoms) Vol. 213 pages 250-254
23. Cirignano L, Glodo J, Gupta T, Higgins WM, Klugerman M, Shah KS, Van Loef E, Wong P Bridgman growth of LaBr/sub3/:Ce and LaCl/sub3/:Ce crystals for high-resolution gamma-ray spectrometers**,** *2006 Vol.287 pp. 239-242*
24. L.L Carter and R.A. Schwarz, MCNP Visual Editor Computer Code Manual, released November, 2005
25. International Basic Safety Standards for Protection against Ionizing Radiation and for the Safety of Radiation Sources, jointly sponsored by FAO, IAEA, OECD/NEA, PAHO, WHO, Vienna, International Atomic Energy Agency, 1996 (IAEA Safety Series, No. 115)
26. Lino Miramonti, A Plastic Scintillator detector for beta particles, Department of physics, Radiation Measurement, University of Milan-INFN, Milano, Italy, Volume 35, Issue 4, August 2002, Pages 347-454.
27. S. Ashrafi, S.M. Etesami, Monte Carlo simulation of plastic scintillator response function in beta-gamma coincidence measurement. Tabriz University, Physics faculty, Tabriz, Iran, Volume 43, Issues 9-10, November 2008.
28. J.S.T.Ng, F.Ryde, S. Rydstrom, T. Takahshi, T.S. Thurston and G. Varner, A Monte Carlo method for calculating the energy response or plastic scintillators to polarized photons below 100 KeV, Hiroshima University, Higashi-Hiroshima, Japan, Volume 600, Issue 3, 11 march 2009, pages 609-617.
29. Raui T. Mainardi, Edgardo V. Bonzi, Monte Carlo calculation of radiation energy absorbed in palsic scintillators, Radiation Physics and Chemistry, Volume 45, Issue 5, May 1995.
30. J. F. Briesmeister, "MCNP-A General Monte Carlo N-Particle Transport Code," LA-12625-M, 1993.
31. David P. Gierga, Electron Photon Calculating using MCNP. Department of Nuclear Engineering, Massachusetts Institute of Technology, 1998.

Appendices

Appendix A: Electron transport in MCNPX

Electron transport is necessarily different from photon transport. Electrons are charged and thus interact continuously through long-range coulomb forces. An electron typically undergoes roughly 10^4 more collisions for the same energy loss than a neutral particle. For example, an electron slowing down from 0.5MeV to 0.0625MeV will undergo on the order of 10^5 collisions. A photon need only undergo about 20-30 Compton scatters to reduce its energy from several MeV to 50keV. Therefore, modeling every electron interaction (analog transport) in a Monte Carlo code is not a viable means of simulating the transport of electrons. Non-trivial problems could not be solved without an enormous investment in computer time. One alternative to analog transport is to follow the electrons over path length (or energy loss) increments that account for the combined effect of multiple collisions, without explicitly modeling every interaction, several multiple-scattering theories have been put forth and attempt to describe the energy loss and angular deflections for electrons. MCNP primarily uses the Bethe-Bloch model for energy loses the Goudsmit-Saunderson theory for angular deflection, the Landau theory of energy straggling, and the Blunck-Leisegang additions to Landau theory. The condensed history algorithm is used in MCNP to transport electrons. In condensed history, multiple scattering theories are applied to a series of steps that combine to equal the electron's complete history. The steps must be chosen such that they are long enough to include enough collisions for the multiple scattering theories to be satisfied, but short enough so the energy loss is small compared t othe kinetic energy of the electron. The multiple scattering distributions are sampled at each step in order to describe the change in the energy and direction of the electron. The seminal reference for the condensed history method

is Marin J. Berger's 1963 paper. Subsequently, Berger and Seltzer developed the ETRAN series of electron-photon transport codes. The Integrated TIGER Series (ITS), a set of general electron-photon transport codes, were formulated using ETRAN as a basis. The electron physics in MCNP mirrors the physics in ITS very closely. (Electron Photon Calculations using MCNP, by David P. Geigra) [31].

Appendix B: Courtesy CANBERRA Co. Website

Argos™-TPS Family of Gasless Whole Body Contamination Monitors

Features

- The Argos-5PB provides the ultimate in (two-step) contoured body coverage
- The Argos-3PB provides contoured body coverage with strategic positioning of detectors to ensure that it outperforms all competitive "economy" model surface contamination monitors (field upgradeable to an Argos-5PB by simply adding the missing detectors)
- Thin Plastic Scintillators have similar performance to gas detectors flow proportional detectors (efficiency, background)
- Individual PMT for each detector allowing optimization of the operating parameters of each detector
- Lowest count times for any given alarm level/background
- Simultaneous monitoring of both sides of the hands with moveable detector for enhanced beta sensitivity
- Ergonomic and very easy-to-use with audible and visible messages on large LCD screen
- Minimal gaps between detectors
- Total front and side access – no need for rear access
- Built-in computer with Windows® XP Embedded operating system with LAN capabilities and USB ports
- Same "industry-best" software and serial bus electronics consistent with CANBERRA Cronos-4/-11 and GEM™-5 monitor families

Description

CANBERRA is proud to introduce the very latest in the Argos line of Whole Body Surface Contamination Monitors. The Argos-5PB and Argos-3PB feature our new gasless, Thin Plastic Scintillator (TPS) detectors whose characteristic parameters have been optimized for the best beta response possible (along with minimizing the gamma response).

To date, the elimination of counting gas has been the only advantage of using of plastic scintillation detectors over traditional gas flow detectors in whole body monitors. The sacrifice for this advantage was in detector performance (low efficiency, bad uniformity) leading to longer count times. Now CANBERRA has successfully addressed the challenges of this gasless detector technology, minimizing the trade-off between operating costs and performance for our customers.

The ARGOS-3/5 PB gasless monitors offer the same industry-best contour geometry as the ARGOS-3/5 AB. The need for counting gas has been eliminated by using scintillation detectors with an embedded PMT to minimize dead space between detectors.

Modern appearance and reliable industrial PC-based operation guarantees employee acceptance and confidence resulting in improved health physics programs, better tracking of contamination and faster, more thorough personnel throughput at boundary points.

Excellent detector protection, modularity of components, and extensive diagnostics result in direct reductions in consumable and work force maintenance costs.

All Argos monitors use a sophisticated "fast following" background trending and release-limit algorithm to provide the best possible performance in stable or varying radiation fields.

OverviewThe TPS detectors in the Argos-PB models are also a brand new design. Their design has been optimized to provide excellent signal-to-noise ratios and furthermore, the detection capability both across and along the detectors is extremely uniform. There is virtually zero edge effect degradation as shown in the uniformity diagram on the next page. The TPS detectors are identical in form factor to the gas detectors from the ARGOS-3/-5AB family. Therefore, the current generation of ARGOS-3/-5AB units can be field upgraded to this latest TPS detector technology*.

The consequence of this improvement in both geometry and detector design is that count times will be significantly reduced compared to other competitive systems.

APPENDIX D ((Courtesy CANBERRA Co.)

The gamma background spectra;

Inline Attachment Follows: CHERNBKGwithEffFromCHERN_Listing.TXT

Aptec PC/MCA - HPS Show June 30-July 3
4/Mar/2010 18:08:40

HEADER INFORMATION in CHERNBKGwithEffFromCHERN.S0 Background, HPS Show, Pitts,PA

Identification
User : Aptec
MCArd : 1
Detector : 1
Geometry : 2
Sample :
Channels : 8192

Acquisition
Started : 2/Jul/1986 12:43:40
Stopped : 2/Jul/1986 13:08:42
True Time : 1500.000 sec
Live Time : 1451.400 sec
Dead Time : 3.24 %
Gross Count : 59112 counts
LTC : 1
Gross Rate : 40.7276 cps

Sample
Sampled 2/Jul/1986 12:43:40

Energy Calibration 12/Dec/1991 18:08:11 CHERNBKG.S0
Resolution Calibration 29/Nov/1991 16:38:44 CHERNBKG.S0
Efficiency Calibration 18/Dec/1991 15:35:16 CHERN.S0
Isotope Library isotope.lib 29/Nov/1991 16:36:36

ACTIVITY INFORMATION for CHERNBKGwithEffFromCHERN.S0 Background, HPS Show, Pitts,PA

Name	Energy keV	Flag	Activity Bq	Error Bq
Bi-214	609.32		28.49	± 6.057
Bi-214	1120.28		32.79	± 20.19
Weighted Average			29.55	± 9.213
Cs-137	661.62		18.94	± 3.823
K-40	1460.75		447.5	± 70.73
Pb-212	238.63		9.709	± 4.285
Pb-214	351.99		25.57	± 5.732
Tl-208	583.14	7	4.995	± 2.074

Grand Total 536.2 ± 71.82

Activity (Bq) at 2/Jul/1986 12:43:40
Errors Quoted at 2 Sigma
MDA's Quoted at 1.645 Sigma

PEAKS NOT IDENTIFIED in CHERNBKGwithEffFromCHERN.S0 Background, HPS Show, Pitts,PA

ROI (#)	Centroid keV	Flag	Net Count Rate cps	Error cps
2	294.82		0.07331	± 0.03055
7	968.73	?	0.01628	± 0.01172

Errors Quoted at 2 Sigma

Flags	Meaning
7	Collect Start to Collect Stop over 7 Half Lives
?	Activity shown is less than MDA value

Inline Attachment Follows: CHERNBKG_Listing.TXT

Aptec PC/MCA - HPS Show June 30-July 3
4/Mar/2010 18:05:47

HEADER INFORMATION in CHERNBKG.S0 Background, HPS Show, Pitts,PA

Identification		Acquisition	
User	: Aptec	Started	: 2/Jul/1986 12:43:40
MCArd	: 1	Stopped	: 2/Jul/1986 13:08:42
Detector	: 1	True Time	: 1500.000 sec
Geometry	: 2	Live Time	: 1451.400 sec
Sample	:	Dead Time	: 3.24 %
Channels	: 8192	Gross Count	: 59112 counts
		LTC	: 1
		Gross Rate	: 40.7276 cps

Sample
Sampled 2/Jul/1986 12:43:40

Energy Calibration 12/Dec/1991 18:08:11 CHERNBKG.S0
Resolution Calibration 29/Nov/1991 16:38:44 CHERNBKG.S0
Isotope Library isotope.lib 29/Nov/1991 16:36:36

NET COUNT RATE INFORMATION for CHERNBKG.S0 Background, HPS Show, Pitts,PA

Name	Energy	Net Count Rate	Error

	keV	Flag	cps	cps
Bi-214	609.32		0.1008	± 0.0207
Bi-214	1120.28		0.01888	± 0.01158
Cs-137	661.62		0.1118	± 0.02169
K-40	1460.75		0.1387	± 0.02019
Pb-212	238.63		0.09278	± 0.04054
Pb-214	351.99		0.1386	± 0.03009
Tl-208	583.14		0.03473	± 0.01429

Errors Quoted at 2 Sigma
MDA's Quoted at 1.645 Sigma

PEAKS NOT IDENTIFIED in CHERNBKG.S0 Background, HPS Show, Pitts,PA

ROI (#)	Centroid keV	Flag	Net Count Rate cps	Error cps
2	294.82		0.07331	± 0.03055
7	968.73	?	0.01628	± 0.01172

Errors Quoted at 2 Sigma

Flags	Meaning
?	Activity shown is less than MDA value

Inline Attachment Follows: CHERN_Listing.TXT

Aptec PC/MCA - HPS Show June 30-July 3
4/Mar/2010 18:01:50

HEADER INFORMATION in CHERN.CHN Turku fallout, Chernobyl+3days

Identification		Acquisition	
User	: Aptec	Started	: 2/Jul/1986 12:14:32
MCArd	: 1	Stopped	: 2/Jul/1986 14:16:21
Detector	: 1	True Time	: 5000.000 sec
Geometry	: 2	Live Time	: 4809.640 sec
Sample	: rag wipe of car	Dead Time	: 3.81 %
Channels	: 8192	Gross Count	: 497672 counts
		LTC	: 1
		Gross Rate	: 103.474 cps

Sample

Sampled 26/Apr/1986 1:23:00
Sample Quantity 1 ± 0 rag
Total Quantity 1 ± 0 rag

Energy Calibration 12/Dec/1991 18:07:02 CHERN.S0
Resolution Calibration 21/Nov/1991 8:50:51 CHERN.S0
Efficiency Calibration 18/Dec/1991 15:35:16 CHERN.S0
Isotope Library isotope.lib 5/Nov/1997 6:31:00

ACTIVITY INFORMATION with FWHM for CHERN.CHN Turku fallout, Chernobyl+3days

Name	Energy keV Library	Energy keV Measured	L - M	FWHM	Flag	Activity pCi	Error pCi
K-40	1460.75	1460.75	-0.00	1.54		1.333e+004	± 1321
Sc-46	889.26	889.16	0.10	0.40		< 30.27	± 1.67
Sc-46	1120.52	1120.66	-0.14	0.53		56.38	± 30.07
Weighted Average						56.38	± 30.07
Zr-95	724.18	724.22	-0.04	1.35		9449.	± 611.3
Zr-95	756.72	756.73	-0.01	1.46		9638.	± 608.7
Weighted Average						9554.	± 610
Nb-95	765.82	765.80	0.02	1.44		1.491e+004	± 870.1
Ru-103	497.08	497.08	-0.00	1.28		3734.	± 238.7
Cs-134	604.66	604.70	-0.04	1.35		515.5	± 71.2
Cs-134	795.84	795.78	0.06	1.46		494.9	± 67.77
Cs-134	801.84	802.17	-0.33	0.67		517.0	± 292.7
Weighted Average						506.4	± 79.54
Cs-137	661.62	661.60	0.02	1.31		1531.	± 129.5
Ba-140	162.64	162.56	0.08	0.81		< 1154.	± 58.61
Ba-140	537.38	537.29	0.09	1.05		876.0	± 374.3
Weighted Average						876.0	± 374.3
Ce-141	145.45	145.45	-0.00	0.95		5621.	± 294.6
Ce-144	80.12	80.28	-0.16	0.87		1.334e+004	± 4607
Ce-144	133.54	133.54	0.00	0.89		1.099e+004	± 698.1
Weighted Average						1.130e+004	± 1138
Ra-226	185.99	186.05	-0.06	0.52		< 1683.	± 95.38
Grand Total						6.142e+004	± 2116

Activity (pCi) at 2/Jul/1986 12:14:32
Errors Quoted at 2 Sigma
MDA's Quoted at 1.645 Sigma

PEAKS NOT IDENTIFIED in CHERN.CHN Turku fallout, Chernobyl+3days

ROI (#)	Centroid keV	FWHM keV	Flag	Net Count Rate cps	Error cps
6	238.63	1.02		0.08533	± 0.02951
7	295.18	0.92		0.05905	± 0.02781
8	328.58	1.05		0.05368	± 0.02542
9	351.96	1.09		0.1264	± 0.02559
10	364.43	0.64	<	0.03329	
11	487.05	0.99		0.1064	± 0.02478
13	511.94	1.04		0.1800	± 0.0272
15	583.27	1.39		0.05674	± 0.01879
17	609.60	1.70		0.1595	± 0.02139
18	622.01	1.33		0.03597	± 0.01493
20	696.39	0.65		0.02857	± 0.0108
26	815.85	0.84		0.02790	± 0.008168
27	852.44	0.83	<	0.005419	
29	911.04	1.18		0.03499	± 0.007573
30	968.95	0.52		0.01079	± 0.006253
31	1119.65	0.27		0.01256	± 0.00512
33	1307.77	0.36	<	0.004444	

Errors Quoted at 2 Sigma

Flags	Meaning
<	MDA value

Appendix E: EJ-212 PLASTIC SCINTILLATOR (Courtesy Eljen Technology)

This is the truly general purpose scintillator suitable for use in geometries ranging from very thin films to thick cast sheet, rods and ingots. EJ-212 is exactly identical to the well-known NE-102A referenced in numerous scientific articles of the past forty years. Applications include industrial and health physics measurement of alpha, beta, gamma and neutron radiation as well as in numerous medical instruments and scientific research ranging from low background shields in nuclear physics to space-borne astrophysics systems.
Since it is formulated for a very wide application range, it is best utilized in sizes up to 100 cm long.
EJ-200 should be considered for longer pieces. The EJ-212 emission spectrum couples well with
common blue-sensitive phototubes and also is sufficiently long to work well with standard acrylic light
guides.
Physical and Scintillation Constants:
Light Output, % Anthracene 65
Scintillation Efficiency, photons/1 MeV e- 10,000
Wavelength of Max. Emission, nm 423
Rise Time, ns ..... ….0.9
Decay Time, ns..... 2.4
Pulse Width, FWHM, ns..... …2.7
No. of H Atoms per cm3, x 1022 ..... 5.17
No. of C Atoms per cm3, x 1022 ..... 4.69
No. of Electrons per cm3, x 1023 ..... 3.33
Density, g/cc: 1.023
Polymer Base: ……. Polyvinyltoluene Light Output vs. Temperature:
Refractive Index: ……1.58 At +60oC, L.O. = 95% of that at +20oC.
Vapor Pressure: …….. Is vacuum-compatible No change from +20oC to -60oC.
Coefficient of Linear
Expansion: ……7.8 x 10-5 below 67oC.
Chemical Compatibility: Is attacked by aromatic solvents, chlorinated solvents, ketones, solvent
bonding cements, etc. It is stable in water, dilute acids and alkalis, lower alcohols and silicone greases. It is safe to use most epoxies and “super glues” with EJ-212.

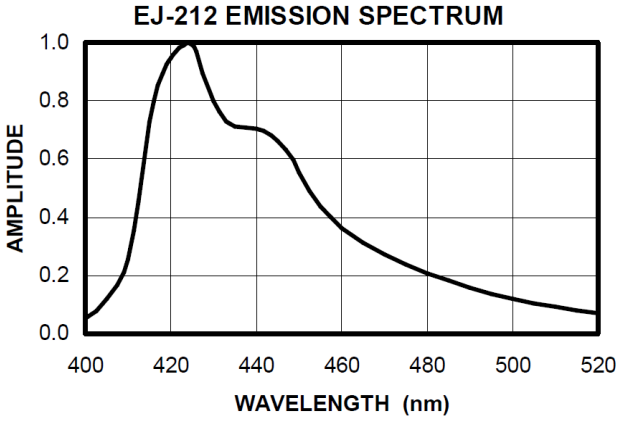
EJ-212 EMISSION SPECTRUM
AMPLITUDE
1.0
0.8
0.6
0.4
0.2
0.0
400
420
440
460
480
500
520
WAVELENGTH (nm)